NACA

RESEARCH MEMORANDUM

INVESTIGATION OF THE LOW-SPEED AERODYNAMIC CHARACTERISTICS OF A VARIABLE-SWEEP AIRPLANE MODEL WITH A TWISTED AND CAMBERED WING

By William B. Kemp, Jr., Robert E. Becht,
and Albert G. Few, Jr.

Langley Aeronautical Laboratory
Langley Field, Va.

NATIONAL ADVISORY COMMITTEE
FOR AERONAUTICS

WASHINGTON

February 1, 1952

NATIONAL ADVISORY COMMITTEE FOR AERONAUTICS

RESEARCH MEMORANDUM

INVESTIGATION OF THE LOW-SPEED AERODYNAMIC CHARACTERISTICS OF A VARIABLE-SWEEP AIRPLANE MODEL WITH A TWISTED AND CAMBERED WING

By William B. Kemp, Jr., Robert E. Becht, and Albert G. Few, Jr.

SUMMARY

An investigation was conducted to determine the low-speed aerodynamic characteristics of a variable-sweep airplane model with a twisted and cambered wing. The wing was designed to have a uniform load distribution at a Mach number 1.10 and a lift coefficient of 0.25 at 50° sweep. A comparison was made with the data obtained on the same model with an untwisted and uncambered wing installed with the same incidence of the mean aerodynamic chord at 50° sweep. The effect of partial-span split flaps was also included in the investigation.

The tests, which were made at a Reynolds number of 2×10^6, based on the mean aerodynamic chord of the 50° swept wing, showed no significantly large changes in lift-curve slope, minimum drag, or longitudinal stability when a twisted and cambered wing was used on the model in place of a flat one of the same geometric plan form. The model with the twisted and cambered wing had higher $(L/D)_{max}$ values at all sweep angles and higher L/D values above the lift coefficient corresponding to $(L/D)_{max}$, especially at low sweep angles. The addition of twist and camber produced a negative increment in the tail-off pitching-moment coefficient at zero lift. This effect, however, was more than counteracted with the tail on by the increased downwash at the tail with the twisted and cambered wing. The use of twist and camber appreciably increased the tail-off $C_{L_{max}}$ of the model, especially at low sweep angles. Moreover, flaps produced as great an increase in the tail-off $C_{L_{max}}$ of the model with the twisted and cambered wing as with the flat wing. The same general trends in lateral and directional stability were obtained with either wing configuration.

[redacted]

INTRODUCTION

The use of swept wings having thin airfoil sections offers promising solutions to some of the aerodynamic problems encountered in high-speed flight. Although wings of this type have low drag at zero lift, objectionably high drag due to lift usually is experienced. Previous investigations at subsonic and supersonic speeds have shown that these lift-drag characteristics could be improved by proper use of twist and camber (references 1 and 2).

The present paper contains the results of an investigation to determine the low-speed longitudinal and lateral stability characteristics of a variable-sweep airplane model having a twisted and cambered wing at four sweep angles with and without trailing-edge flaps. A comparison also is made with the data presented in references 3 and 4 for the same model but with an untwisted and uncambered wing of the same geometric plan form.

SYMBOLS

The system of axes employed, together with an indication of the positive forces, moments, and angles, is given in figure 1. The aerodynamic force and moment coefficients are based on the actual wing area and span which vary with sweep angle, but a constant chord, equal to the wing mean aerodynamic chord at 50° sweep, is used for the pitching-moment coefficient. The symbols used are defined as follows:

C_L	lift coefficient (Lift/qS)
C_X	longitudinal-force coefficient (X/qS)
C_{D_o}	wing profile-drag coefficient
C_Y	lateral-force coefficient (Y/qS)
C_l	rolling-moment coefficient (L/qSb)
C_m	pitching-moment coefficient ($M/qS\bar{c}_{50}$)
C_n	yawing-moment coefficient (N/qSb)
X	longitudinal force along X-axis (Drag = -X), pounds
Y	lateral force along Y-axes, pounds

Z	force along Z-axes (Lift = -Z), pounds
L	rolling moment about X-axes, foot-pounds
M	pitching moment about Y-axes, foot-pounds
N	yawing moment about Z-axes, foot-pounds
q	free-stream dynamic pressure, pounds per square foot ($\rho V^2/2$)
q_t	effective dynamic pressure at the tail, pounds per square foot
ϵ	effective downwash angle at tail, degrees
S	wing area, square feet
$\bar{c}$	wing mean aerodynamic chord, feet (based on plan forms shown in fig. 2)
$\bar{c}_{50}$	wing mean aerodynamic chord at 50° sweep, feet
c'	local streamwise wing chord, feet
c	local wing chord perpendicular to quarter-chord line of unswept wing, feet
b	wing span, feet
V	free-stream velocity, feet per second
A	aspect ratio (b^2/S)
ρ	mass density of air, slugs per cubic foot
α	angle of attack of thrust line, degrees
ψ	angle of yaw, degrees
i_t	angle of incidence of stabilizer with respect to thrust line, degrees
δ_f	flap deflection measured in a plane perpendicular to hinge line, degrees
	angle of sweepback of quarter-chord line of unswept wing, degrees

y spanwise distance measured perpendicular from plane of symmetry, feet

h distance above chord plane, feet

d streamwise distance back of local wing leading edge, feet

Subscript:

ψ denotes partial derivative of a coefficient with respect to yaw (example: $C_{l_\psi} = \partial C_l / \partial \psi$)

APPARATUS AND METHODS

Description of Model

The model used in the present investigation was the same as that used in the tests of references 3 and 4, with the exception of the wing. The wing was replaced by one that incorporated camber and twist. The physical characteristics of the model are presented in figure 2 and photographs of the model on the support strut are given as figure 3. Figure 4 shows details of the split flap. The model was constructed of wood bonded to steel reinforcing members.

The wing mean surface was designed by the method of reference 5 to produce a uniform load distribution at a Mach number of 1.10 and a lift coefficient of 0.25 at 50° sweep. The twist of this surface was modified inboard of the 23-percent-semispan station to avoid the infinite twist at the root indicated by the theoretical derivation. The derivation of the actual mean surface used is described in more detail in reference 2. Plots of the spanwise distribution of maximum camber, location of maximum camber, and streamwise twist angle are presented in figures 5, 6, and 7, respectively. The thickness distribution measured in planes normal to the 0.25-chord line of the unswept wing was NACA $64_{(10)}$A010.3 at the root tapering to NACA 64A008 at the tip.

The wings were pivoted about axes parallel to the plane of symmetry and normal to the mean aerodynamic chord at 50° sweep so that the swept-back angle could be varied continuously from 20° to 60°. The wing incidence measured in a streamwise direction was zero, as was that of the flat wing, at the mean aerodynamic chord at 50° sweep. At all sweep angles, the wing was located so that the quarter chord of the mean aerodynamic chord fell at a fixed fuselage station. The moment reference center was located at this same fuselage station. (See fig. 2.)

[redacted]

A jet-engine duct was simulated on the model by use of an open tube having an inside diameter equal to that of the jet exit and extending from the nose to the jet exit.

TESTS

The tests were made in the Langley 300 MPH 7- by 10-foot tunnel at a dynamic pressure of 34.15 pounds per square foot which corresponds to a Mach number of 0.152 and a Reynolds number of 2×10^6, based on the mean aerodynamic chord of the wing at 50° sweep for average test conditions.

During the tests no control was imposed on the air-flow quantity through the jet duct. Measurements made in previous tests indicated that the inlet-velocity ratio varied between 0.78 and 0.86, the higher values being observed at low angles of attack.

Two types of tests were employed for determining the lateral characteristics of the model. The parameters, C_{n_ψ}, C_{y_ψ}, and C_{l_ψ}, were determined from tests through the angle-of-attack range at yaw angles of 0° and 5°. The lateral characteristics were also determined from tests through a range of yaw angles at constant angle of attack. Flow surveys at several angles of attack were made behind the twisted and cambered 50° swept-wing configuration to determine the dynamic pressure and effective downwash at the tail. The surveys were made in planes perpendicular to the tail mean aerodynamic chord and passing through the 0.25-mean-aerodynamic-chord point of the horizontal tail and 6 inches behind this point.

CORRECTIONS

The angle-of-attack, drag, and pitching-moment results have been corrected for jet-boundary effects computed on the basis of unswept-wing theory by the method of reference 6. Calculations have shown that the effects of sweep on these corrections are negligible. All coefficients have been corrected for blocking due to the model and its wake by the method of reference 7.

Corrections for the tare forces and moments produced by the support strut have not been applied. It is probable, however, that the significant tare corrections would be limited to small increments in pitching moment and drag.

[redacted]

Vertical buoyancy on the support strut, tunnel air-flow misalinement, and the longitudinal-pressure gradient have been accounted for in computation of the test data.

RESULTS AND DISCUSSION

Presentation of Results

The results of the investigation are presented in the figures listed below:

	Figure No.
Longitudinal aerodynamic characteristics	8
Drag characteristics	9 to 10
Lift-drag ratios	11 to 12
Pitching-moment characteristics	13
Dynamic pressure and downwash at tail	14 to 15
Effect of flaps	16 to 17
Lateral and directional stability characteristics	18 to 19

In order to provide a comparison which will indicate the effects of camber and twist, data from references 3 and 4 on the untwisted, uncambered wing model (hereinafter referred to as the flat-wing model) are included in some of the figures. As was pointed out in the section on symbols, the aerodynamic coefficients presented herein are based on the wing area and span of the sweep configuration in question and on the mean aerodynamic chord of the wing at 50° sweep. Thus, the pitching-moment coefficients are based on a reference length which is fixed with respect to the fuselage and is independent of sweep angle; whereas all other coefficients are of the usual form.

Lift Characteristics

A comparison of the tail-off lift curves of figure 8 with those presented in reference 3 for the flat-wing model indicated that no significant changes in lift-curve slope were produced by twisting and cambering the wing. The use of twist and camber, however, reduced the angle of attack corresponding to zero lift approximately 4° at 20° sweep and approximately 1° at 60° sweep. This reduction with increasing sweep of the effect of twist and camber on the angle of zero lift, as well as on other characteristics to be discussed subsequently, resulted primarily from the reduction with sweep of the effective amount of camber (fig. 5) and twist (fig. 7) incorporated in the wing.

[redacted]

The summary of maximum lift coefficients presented in figure 17 shows that the maximum lift coefficient of the flat-wing model increased considerably with increasing sweep. The effect of camber and twist was to increase the maximum lift coefficient by an amount which decreased with increasing sweep. The resulting values of maximum lift coefficient showed a much smaller variation with sweep angle than those for the flat wing.

Drag Characteristics

A comparison of the tail-off drag polars of the flat wing and the twisted and cambered wing models is presented in figure 9. The drag at zero lift of the twisted and cambered wing model was slightly higher at all sweep angles than that obtained with the flat wing. The magnitude of the drag difference, however, decreased with increasing sweep.

At the lower sweep angles, large increases in drag coefficient with increasing lift coefficient were observed only at lift coefficients near the maximum. The addition of camber and twist increased the maximum lift coefficient and thus increased the lift corresponding to a rapid increase in drag. At sweep angles of 50° and 60°, tuft observations on the flat-wing model indicated that leading-edge separation occurred at moderate and high lift coefficients. Incorporating camber and twist would be expected to delay this separation to higher lift coefficients by reducing the magnitude of the negative pressure peaks on the leading edge. The resulting drag reduction over a wide range of lift coefficients is evident in figures 9(c) and 9(d).

Inasmuch as the benefits of twist and camber result to some extent from their effect on flow separation, it is anticipated that these benefits would be dependent on Reynolds number. The evidence available at present (for example, references 8 and 9) shows that the effects of twist and camber may either increase or decrease with increasing Reynolds number. Thus, caution should be exercised in applying the results of the present investigation to full-scale flight conditions.

Figure 10 presents the wing profile drag for both model configurations. These data were obtained by subtracting the theoretical induced drag for an assumed elliptic spanwise loading $\left(\frac{C_L^2}{\pi A}\right)$ and the fuselage-alone drag from the total experimental drag of the wing-fuselage combination. No allowance was made for the wing-fuselage interference effects. The profile drag coefficient at all sweep angles of the twisted and cambered wing decreased from zero-lift value to a minimum at some intermediate lift coefficient; whereas, the flat-wing profile drag generally increased with lift coefficient from the zero-lift value. A similar behavior in

[redacted]

the profile-drag variation with lift coefficient of another twisted and cambered wing model was reported in reference 1 and is usually apparent in the section characteristics of cambered airfoil sections. The lift coefficient corresponding to minimum profile drag decreased with increasing sweep. The beneficial effect of twist and camber at the higher lift coefficients observed in figure 9 is also apparent in the profile-drag characteristics of figure 10.

Lift-Drag Ratio

The variation of $(L/D)_{max}$ with sweep angle presented in figure 11 indicates that the twisted and cambered wing model had higher values of $(L/D)_{max}$ than those obtained for the flat-wing model at all sweep angles investigated. The increases in $(L/D)_{max}$ were 2.2, 2.4, 16.5, and 14.1 percent for the configurations with 20°, 35°, 50°, and 60° wing sweep, respectively. The effect of twist and camber on the variation of L/D with lift coefficient is presented in figure 12. At 20° wing sweep, higher values of L/D were obtained for the flat-wing configuration than for the twisted and cambered wing configuration at all lift coefficients up to very nearly the lift coefficient corresponding to $(L/D)_{max}$. Similar trends were also observed in the 35°-wing-sweep configuration although the difference in the (L/D) values was not so great. Above the lift coefficient corresponding to $(L/D)_{max}$, the twisted and cambered wing model, especially with 20° wing sweep, exhibited much higher L/D values than were obtained for the flat-wing model. This improvement may be attributed to the decreased C_{D_o} and the increased $C_{L_{max}}$ previously noted.

Pitching-Moment Characteristics

A comparison of the tail-off pitching-moment-coefficient curves for both models presented in figure 13 shows that the addition of twist and camber produced essentially no change in static longitudinal stability in the low-lift-coefficient range. For sweep angles of 50° and 60°, as the lift coefficient was increased, an increase in stability was observed and was followed by a stability decrease near $C_{L_{max}}$. This characteristic is typical of that usually observed with thin, highly swept wings. The effect of twist and camber was to increase the lift coefficients at which these stability changes occurred.

Figure 13 also indicates that the twisted and cambered wing model produced pitching-moment coefficients at zero lift which were considerably more negative than those for the flat wing, especially at low sweep angles.

[redacted]

The contribution of camber alone was estimated from section data to be -0.060 at 20° sweep and -0.033 at 60° sweep. Data presented in reference 3 for the fuselage alone indicated that, at the angles of attack corresponding to zero lift of the twisted and cambered wing model, the fuselage pitching-moment coefficients were -0.020 at 20° sweep and -0.006 at 60° sweep. The wing twist, which would be expected to produce positive pitching-moment increments, was apparently not large enough to counteract the combined effects of camber and fuselage attitude on the zero-lift pitching-moment coefficients.

Dynamic Pressure and Downwash at Tail

The ratio of dynamic pressure at the tail to free-stream dynamic pressure q_t/q and the downwash at the tail were calculated from the measured pitching-moment characteristics of figure 8 and are presented in figures 14 and 15, respectively. Results of tests of the fuselage and tail combination were used to represent the isolated tail characteristics.

The data of figure 14 show that unreasonably high values of q_t/q were obtained throughout the sweep range at relatively high angles of attack for the twisted and cambered wing model. Flow surveys, therefore, were made in the vicinity of the horizontal tail with the wing at 50° sweep, and the results were integrated over the tail area as a check on the calculated values of q_t/q and downwash. Fairly good agreement between the calculated and measured values of q_t/q and downwash was obtained only at angles of attack less than 16°. The discrepancies observed at higher angles of attack are attributed largely to the combined effects of the tail sweepback and a vertical gradient of downwash associated with the pattern of flow separation from the wing at high angles of attack. With the swept tail, a change in tail incidence produced a vertical translation of sections of the tail, especially near the tips. This translation combined with a vertical gradient of downwash produced a change in tail angle of attack which, in the present case, added to the change in tail incidence. The resulting high tail effectiveness produced the erroneously high values of calculated q_t/q and downwash angle.

Figure 15 indicates that the addition of twist and camber had essentially no effect on the rate of change of downwash with angle of attack although the absolute values of downwash angle were higher for the twisted and cambered wing than for the flat wing. The increase in downwash angle became smaller with increasing sweep and probably resulted primarily from the twist of the inboard part of the wing. As shown in figure 7, the twist also decreased with increasing sweep. A comparison of the tail-on pitching-moment coefficients of figure 8 with those of reference 3 showed that this increase in downwash angle was large enough

so that, for a given tail incidence, the zero-lift pitching-moment coefficients became more positive with the addition of twist and camber although the tail-off pitching-moment coefficients became more negative.

Effect of Flaps

The longitudinal aerodynamic characteristics of the twisted and cambered wing model with a split flap deflected 50° are presented in figure 16 for sweep angles of 20°, 35°, and 50°. The flap, details of which are given in figure 4, was identical in plan form with flap B of reference 3.

A comparison of figures 8 and 16 indicates that, at a lift coefficient of 0.5 which may be representative of the point at which flaps would be deflected, only small changes in static longitudinal stability accompanied flap deflection. The negative increment of pitching-moment coefficient produced by flap deflection at $C_L = 0.5$ reached values as high as 0.080 with the horizontal tail off. For the complete model, however, the additional downwash behind the flap reduced this increment to a maximum of 0.020.

The summary of tail-off maximum lift coefficients presented in figure 17 indicates that, although appreciable increases in $C_{L_{max}}$ were produced by twist and camber, the increment in $C_{L_{max}}$ produced by the flaps was essentially the same for the twisted and cambered wing as for the flat wing. The increment in $C_{L_{max}}$ produced either by flap deflection or by twist and camber suffered a marked reduction as the sweep angle was increased.

Lateral Stability Characteristics

Figure 18 presents a comparison of the lateral stability parameters for the twisted and cambered wing model and the flat wing model. The characteristics in yaw of the twisted and cambered wing model are presented in figure 19. Except for differences in absolute values, the same general trends in directional stability and effective dihedral obtained on the flat wing (see reference 4) were also evidenced on the twisted and cambered wing model. The directional instability observed at high lift coefficients was attributed in reference 4 to mutual interference between the wing, fuselage, and tail. Although directional instability occurred at a higher lift coefficient on the twisted and cambered wing model, the incremental difference between the lift coefficient for stall and the lift coefficient at which directional instability occurred was approximately the same for both model configurations.

[redacted]

Significant increases in directional stability were observed on the twisted and cambered wing model at low and negative lift coefficients at 35° and 50° sweep. Similar trends were observed in the lateral-force coefficient slope C_{y_ψ} and indicated that the increases in directional stability were probably produced by changes in sidewash at the tail.

The effective dihedral of the twisted and cambered wing was greater than that of the flat wing at all wing sweep angles except 60°. The values of effective dihedral obtained from pitch tests at yaw angles of 0° and 5° of the twisted and cambered wing model with 50° and 60° sweep appeared to be in error and are, therefore, not presented. The values appearing in figures 18(c) and 18(d) for the twisted and cambered wing were obtained from the yaw test data of figure 19.

CONCLUSIONS

Results of an investigation at low speed of the aerodynamic characteristics of a variable-sweep airplane model with a twisted and cambered wing compared with the results obtained for the model with a flat wing of the same geometric plan form indicate the following conclusions:

1. No significantly large changes in lift-curve slope, minimum drag, or longitudinal stability were observed when a twisted and cambered wing was used on the model in place of a flat wing.

2. The model with the twisted and cambered wing had higher $(L/D)_{max}$ values at all sweep angles and higher L/D values above the lift coefficient corresponding to $(L/D)_{max}$ especially at low sweep angles.

3. The addition of twist and camber produced a negative increment in the tail-off pitching-moment coefficient at zero lift. This effect was more than counteracted with the tail on, however, by the increased downwash at the tail with the twisted and cambered wing.

4. The use of twist and camber appreciably increased the tail-off $C_{L_{max}}$ of the model, especially at low sweep angles. Moreover, flaps produced as great an increase in the tail-off $C_{L_{max}}$ of the model with the twisted and cambered wing as with the flat wing.

[redacted]

5. The same general trends in lateral and directional stability were obtained with either wing configuration.

Langley Aeronautical Laboratory
National Advisory Committee for Aeronautics
Langley Field, Va.

REFERENCES

1. Weiberg, James A., and Carel, Hubert C.: Wind-Tunnel Investigation at Low Speed of a Wing Swept Back 63° and Twisted and Cambered for a Uniform Load at a Lift Coefficient of 0.5. NACA RM A50A23, 1950.

2. Spreeman, Kenneth P., and Alford, William J., Jr.: Investigation of the Effects of Twist and Camber on the Aerodynamic Characteristics of a 50° 38' Sweptback Wing of Aspect Ratio 2.98. Transonic-Bump Method. NACA RM L51C16, 1951.

3. Kemp, William B., Jr., Becht, Robert E., and Few, Albert G., Jr.: Stability and Control Characteristics at Low Speed of a $\frac{1}{4}$-Scale Bell X-5 Airplane Model. Longitudinal Stability and Control. NACA RM L9K08, 1950.

4. Kemp, William B., Jr., and Becht, Robert E.: Stability and Control Characteristics at Low Speed of a $\frac{1}{4}$-Scale Bell X-5 Airplane Model. Lateral and Directional Stability and Control. NACA RM L50C17a, 1950.

5. Jones, Robert T.: Estimated Lift-Drag Ratios at Supersonic Speed. NACA TN 1350, 1947.

6. Gillis, Clarence L., Polhamus, Edward C., and Gray, Joseph L., Jr.: Charts for Determining Jet-Boundary Corrections for Complete Models in 7- by 10-Foot Closed Rectangular Wind Tunnels. NACA ARR L5G31, 1945.

7. Herriot, John G.: Blockage Corrections for Three-Dimensional-Flow Closed-Throat Wind Tunnels, with Consideration of the Effect of Compressibility. NACA Rep. 995, 1950. (Formerly NACA RM A7B28.)

8. Tinling, Bruce E., and Kolk, W. Richard: The Effects of Mach Number and Reynolds Number on the Aerodynamic Characteristics of Several 12-Percent-Thick Wings Having 35° of Sweepback and Various Amounts of Camber. NACA RM A50K27, 1951.

9. Johnson, Ben H., Jr., and Shibata, Harry H.: Characteristics throughout the Subsonic Speed Range of a Plane Wing and of a Cambered and Twisted Wing, Both Having 45° of Sweepback. NACA RM A51D27, 1951.

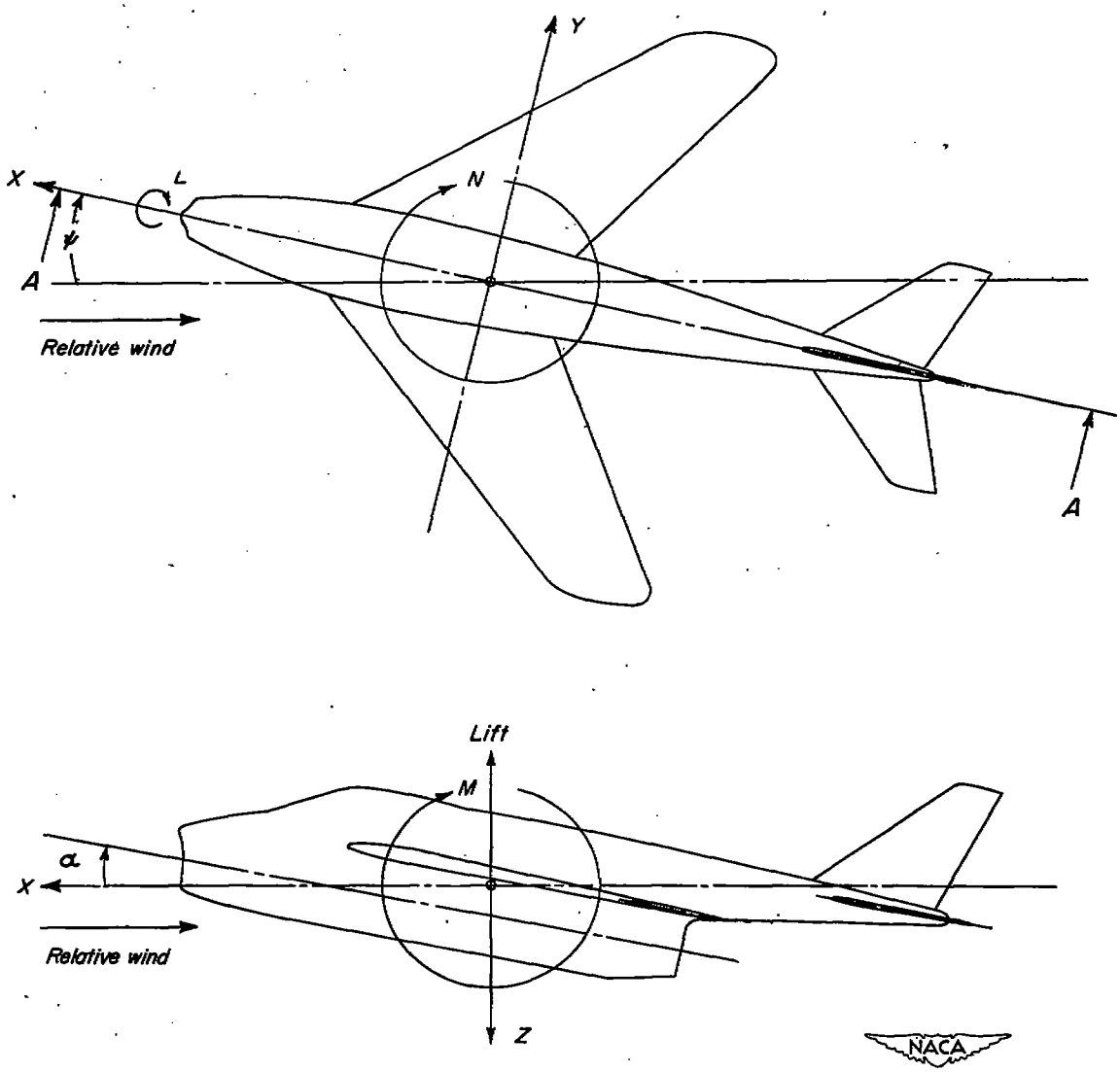

View A-A

Figure 1.- System of axes. Positive values of forces, moments and angles are indicated by arrows.

[redacted]

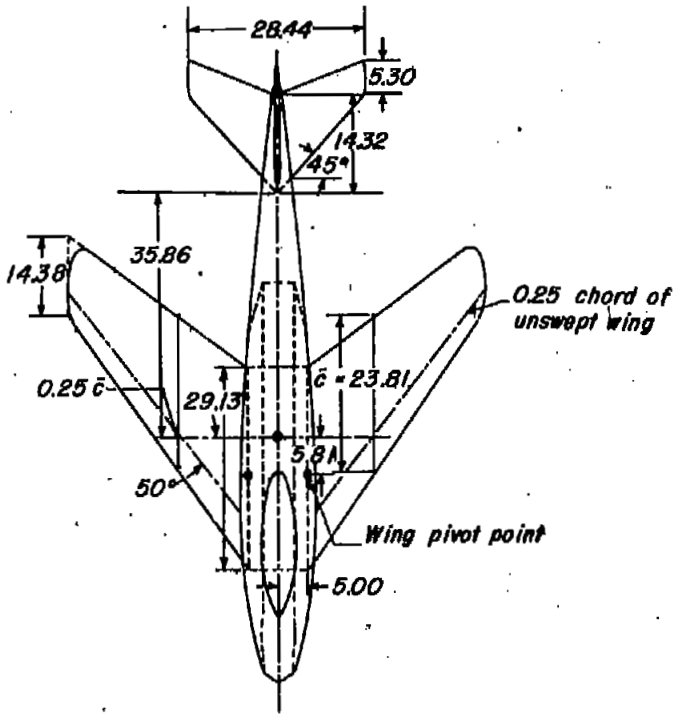

Physical characteristics

Wing

Sweep, deg	20	35	50	60
Area, sq ft	10.33	10.45	10.80	11.33
Aspect ratio	5.76	4.56	2.98	1.92
Span, ft	7.72	6.90	5.67	4.66
Mean aerodynamic chord, ft	1.396	1.579	1.985	2.535
Incidence at M.A.C., deg	0.60	0.25	0	0.10
Dihedral, deg	-2	-2	-2	-2

Horizontal tail

Area, sq ft	1.94
Aspect ratio	2.89

Vertical tail

Area, sq ft	1.33
Aspect ratio	1.46

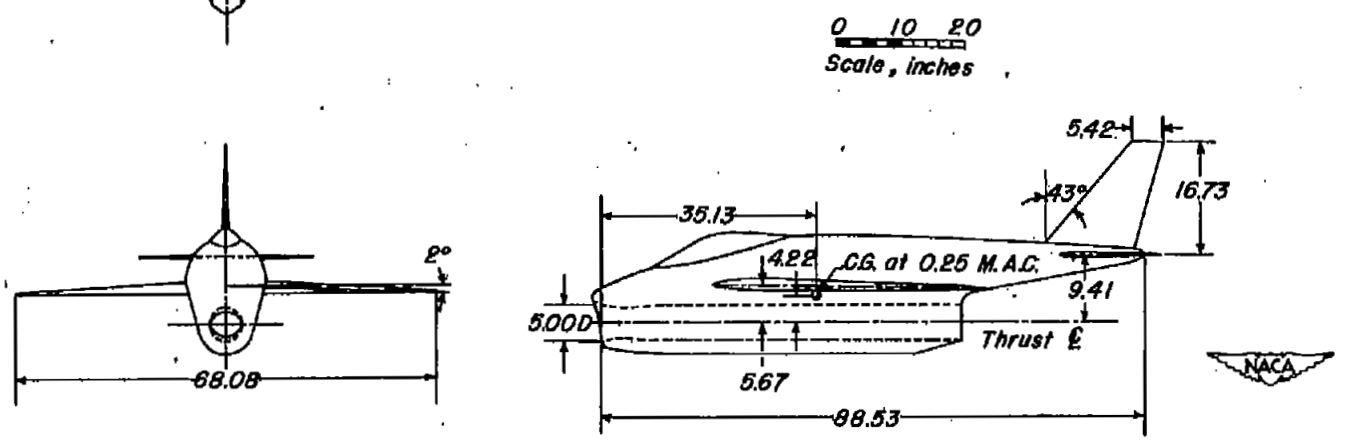

Figure 2.- General arrangement of test model.

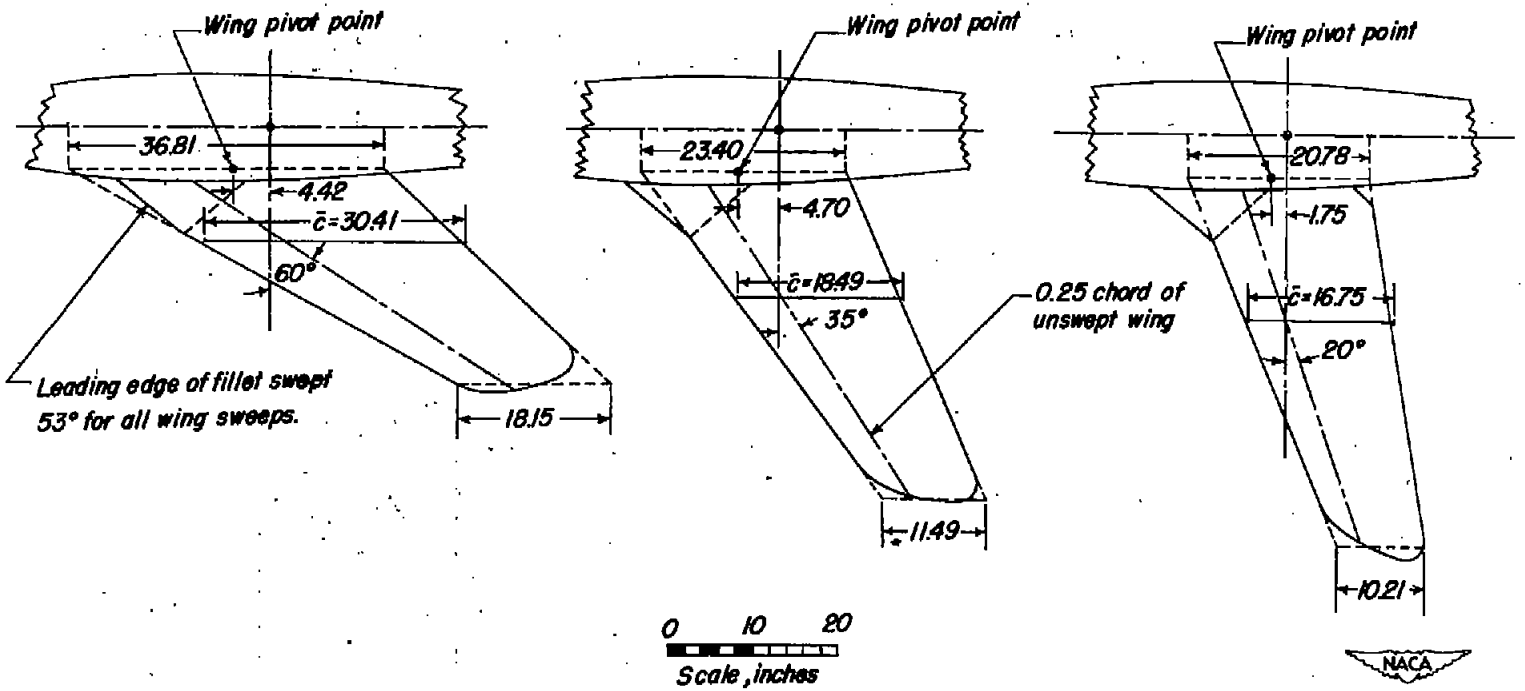

Figure 2.- Concluded.

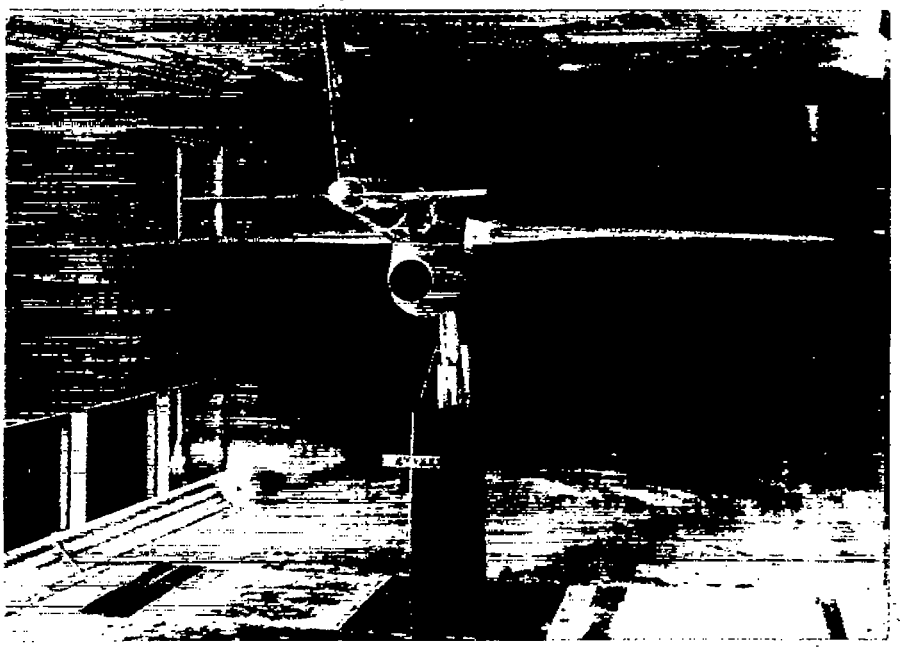

(a) Rear view.

NACA L-65810

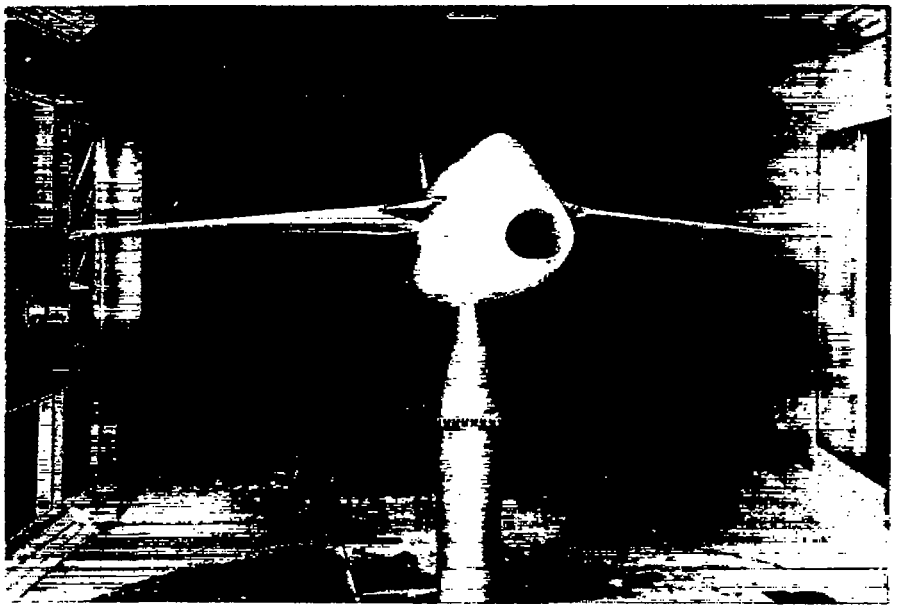

(b) Front view.

NACA L-65808

Figure 3.- Views of test model as mounted in tunnel.

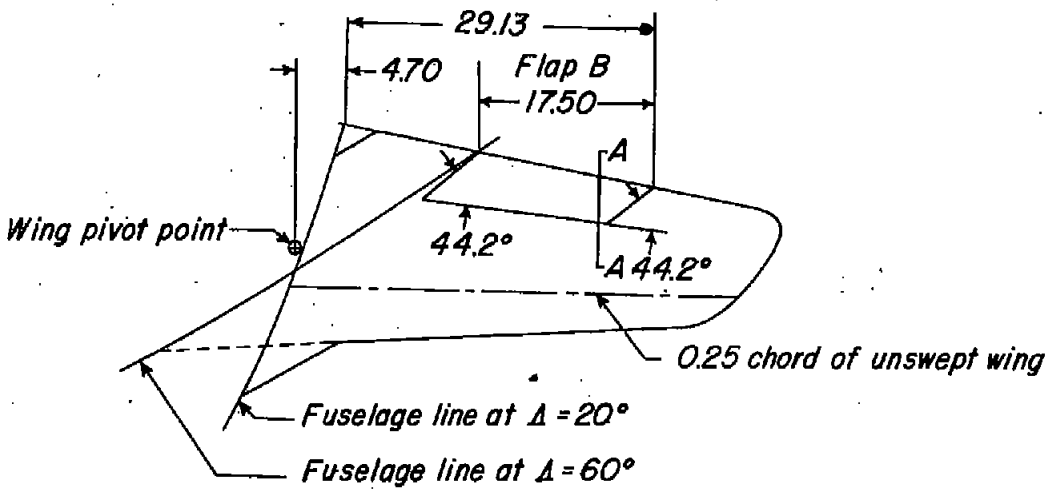

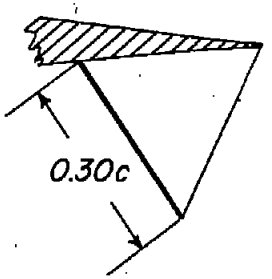

Section A-A

Figure 4.- Details of split flap.

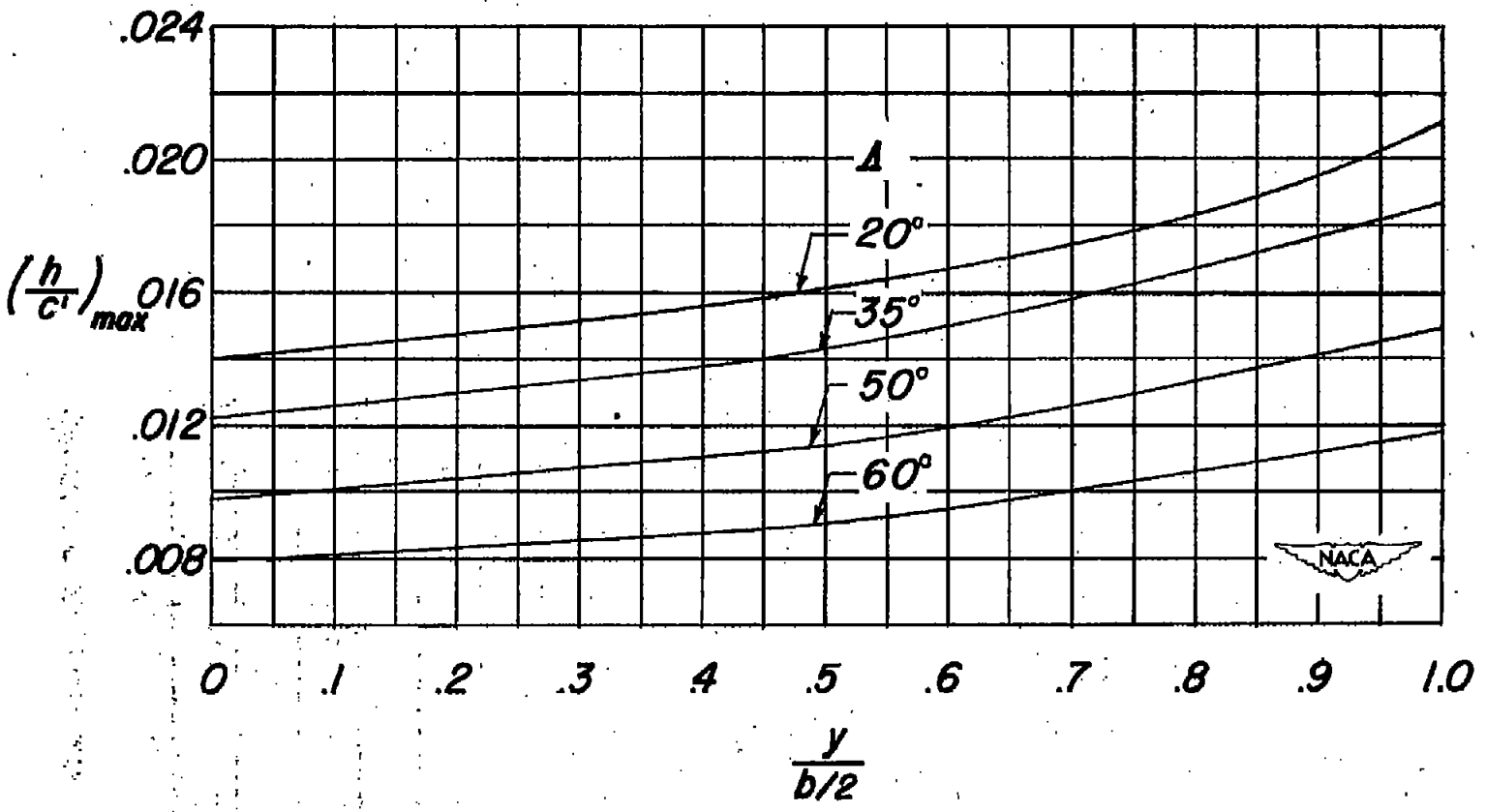

Figure 5.- Spanwise distribution of maximum camber.

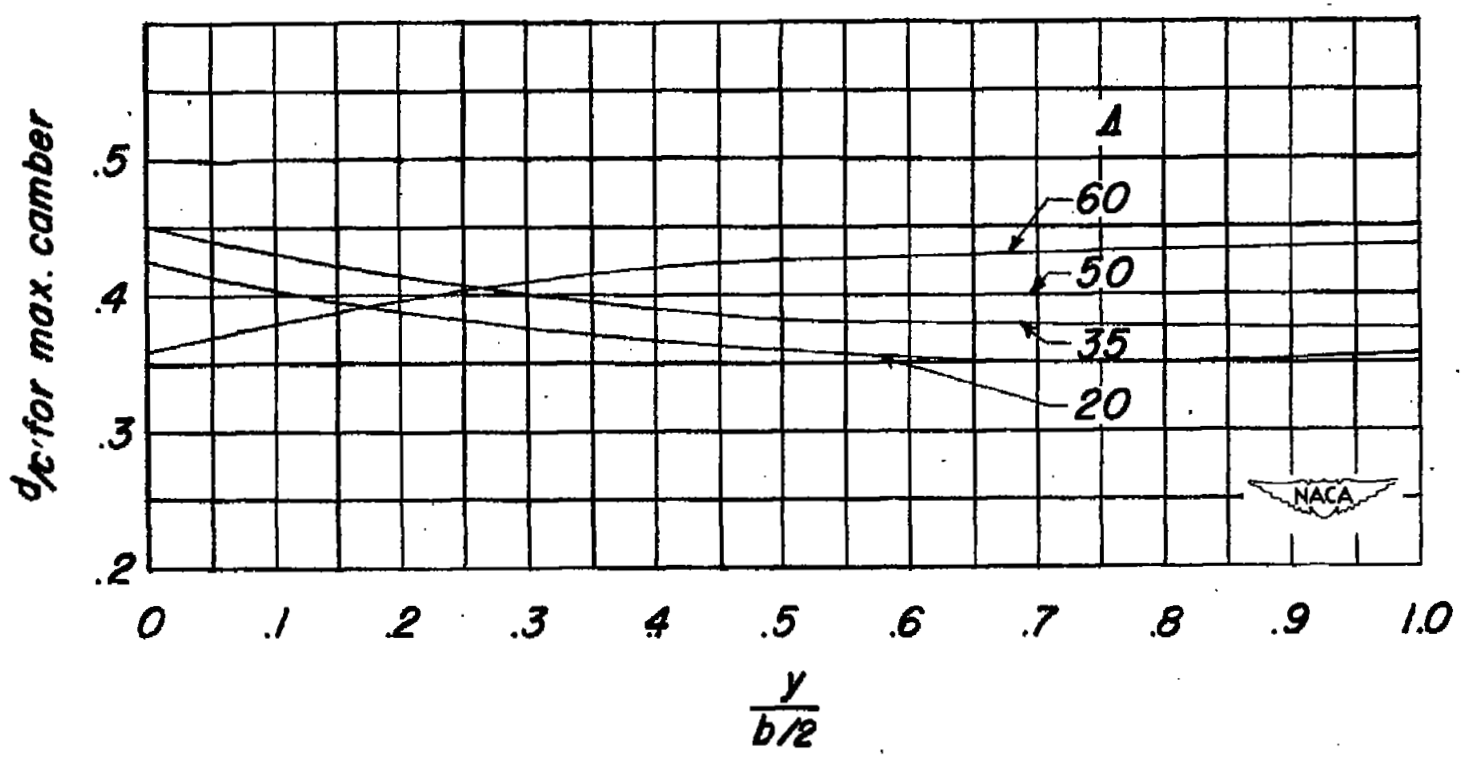

Figure 6.- Chordwise location of maximum camber.

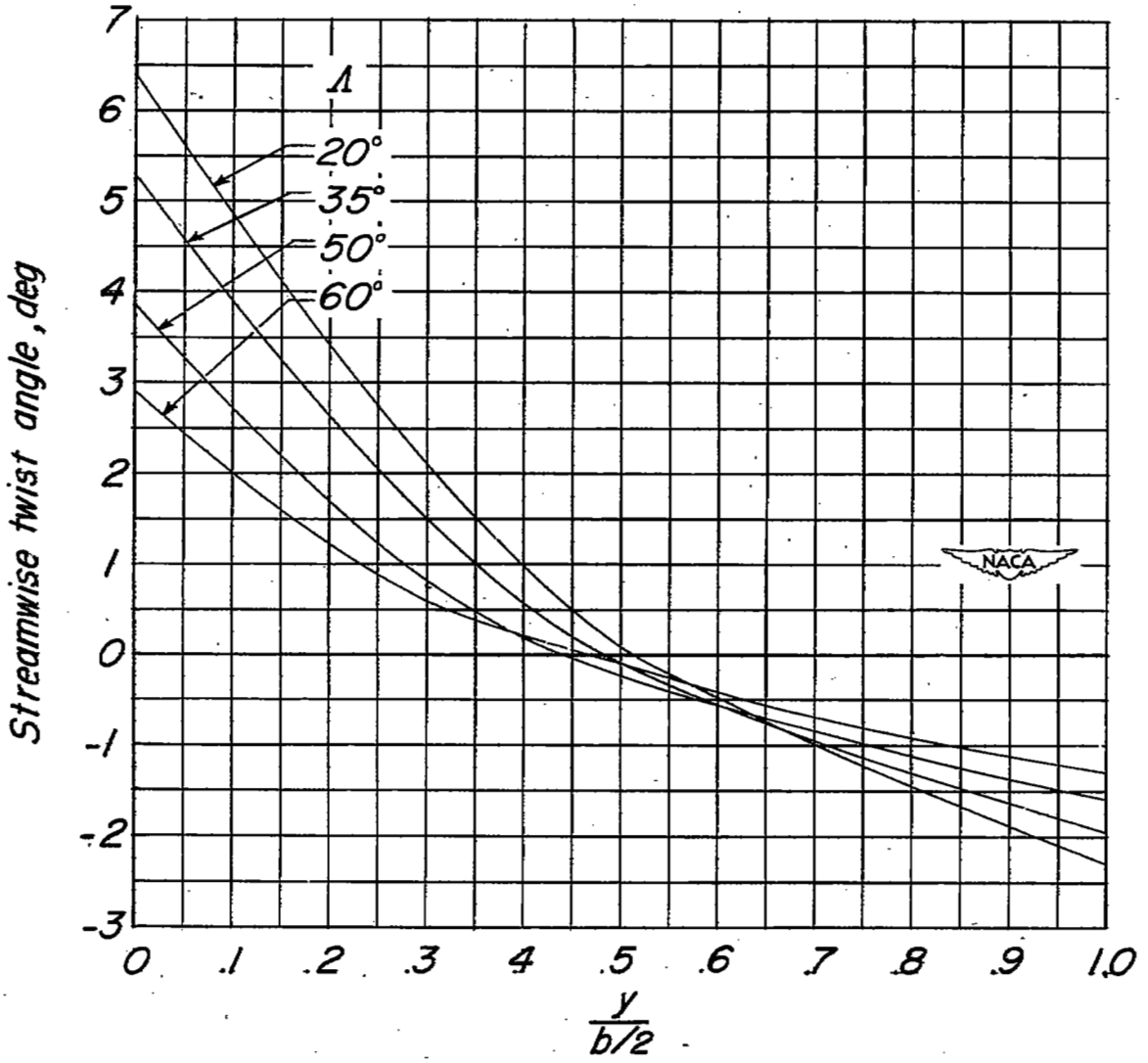

Figure 7.- Spanwise distribution of streamwise twist angle.

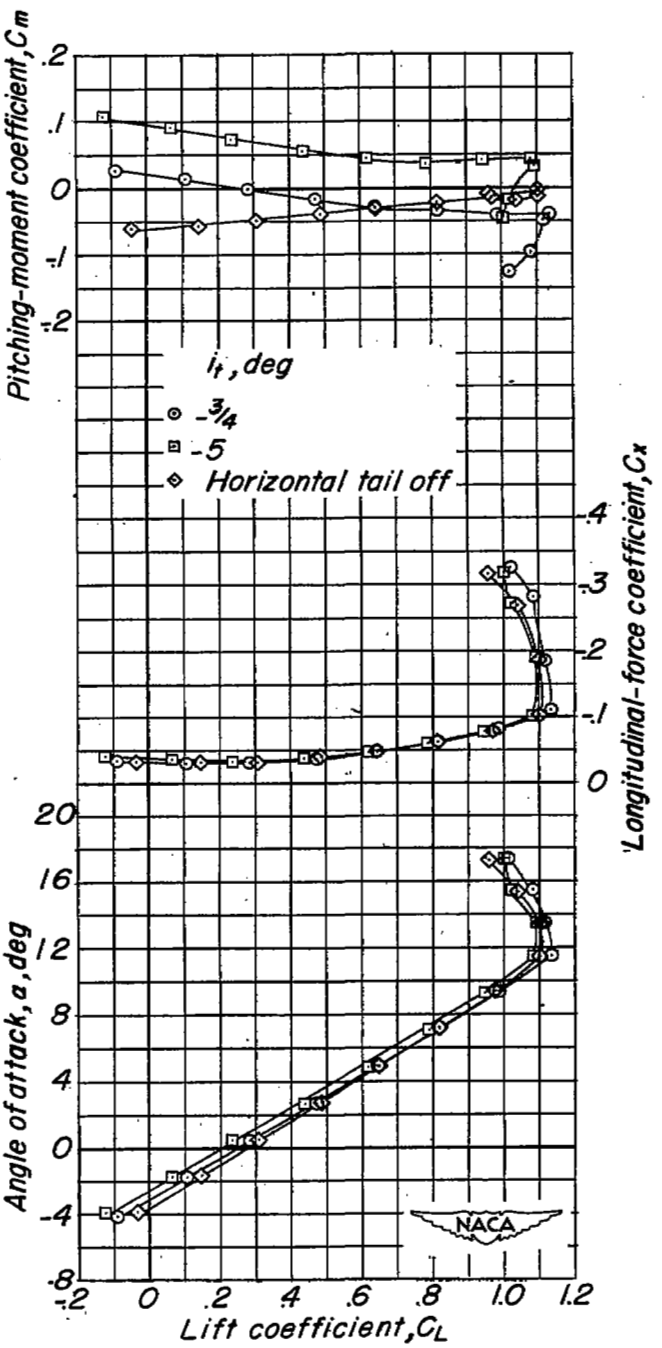

(a) $\Lambda = 20^\circ$.

Figure 8.- The longitudinal aerodynamic characteristics of the twisted and cambered wing model. $\delta_f = 0^\circ$.

[redacted]

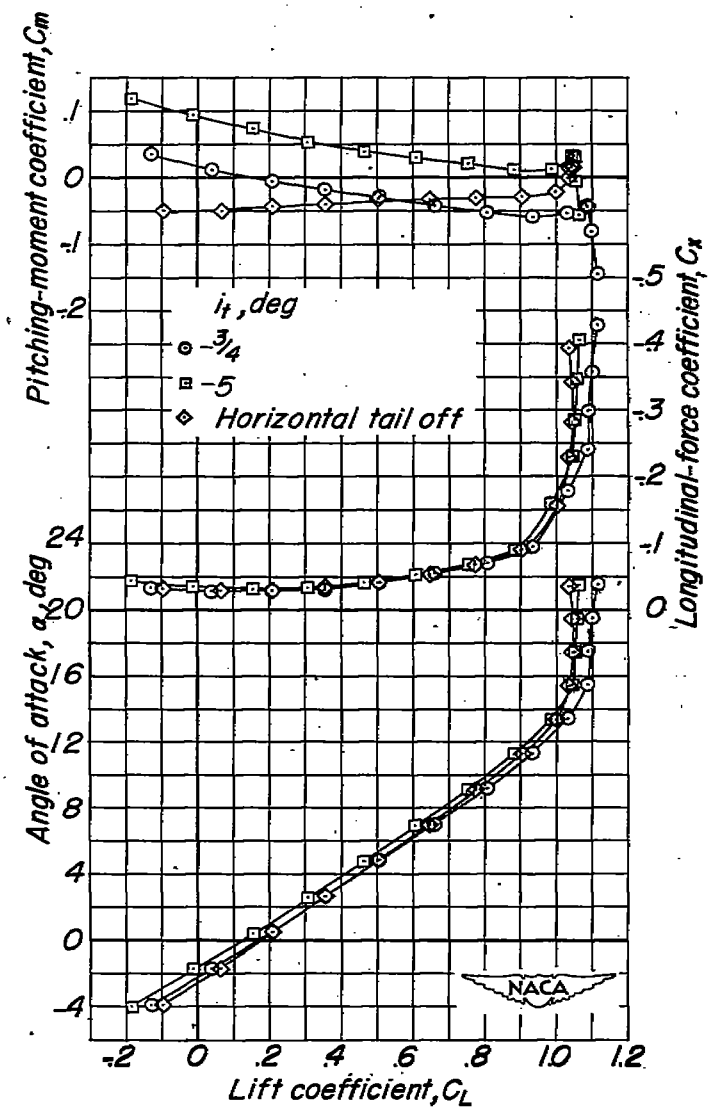

(b) $\Lambda = 35°$.

Figure 8.- Continued.

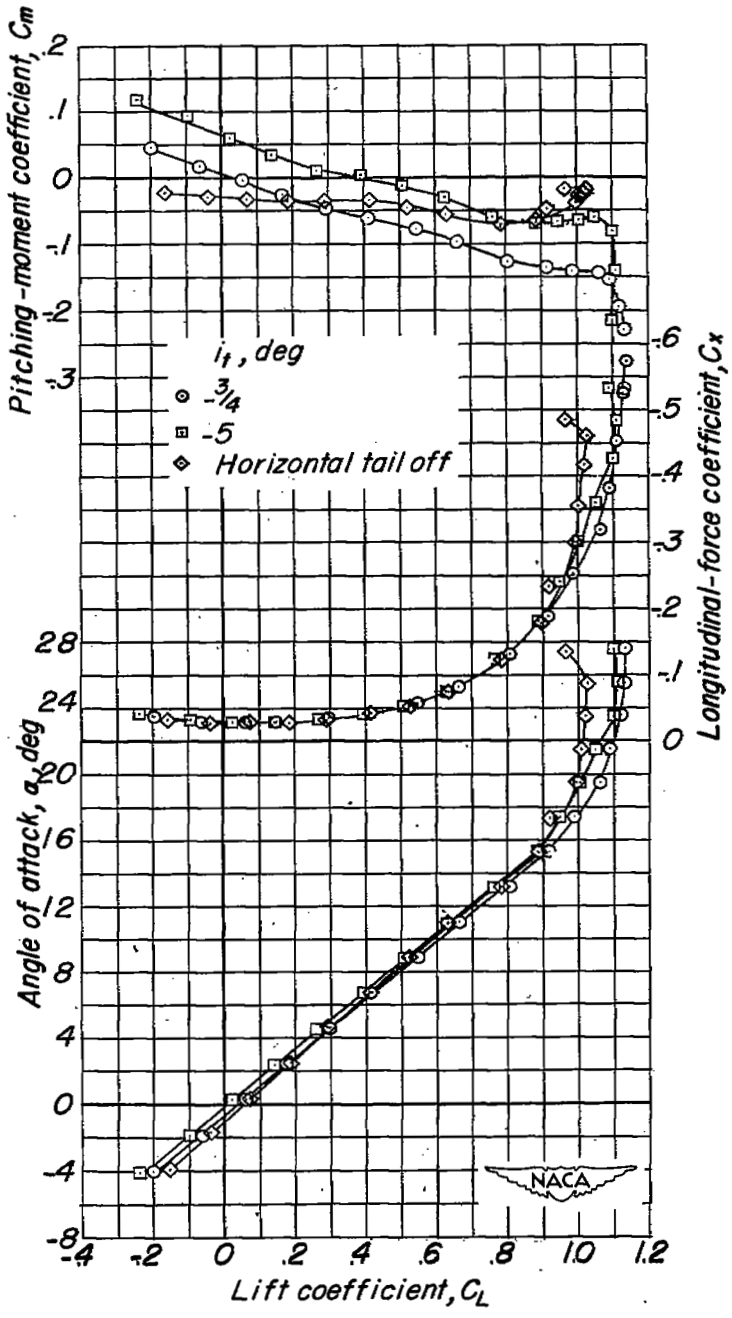

(c) $\Lambda = 50°$.

Figure 8.- Continued.

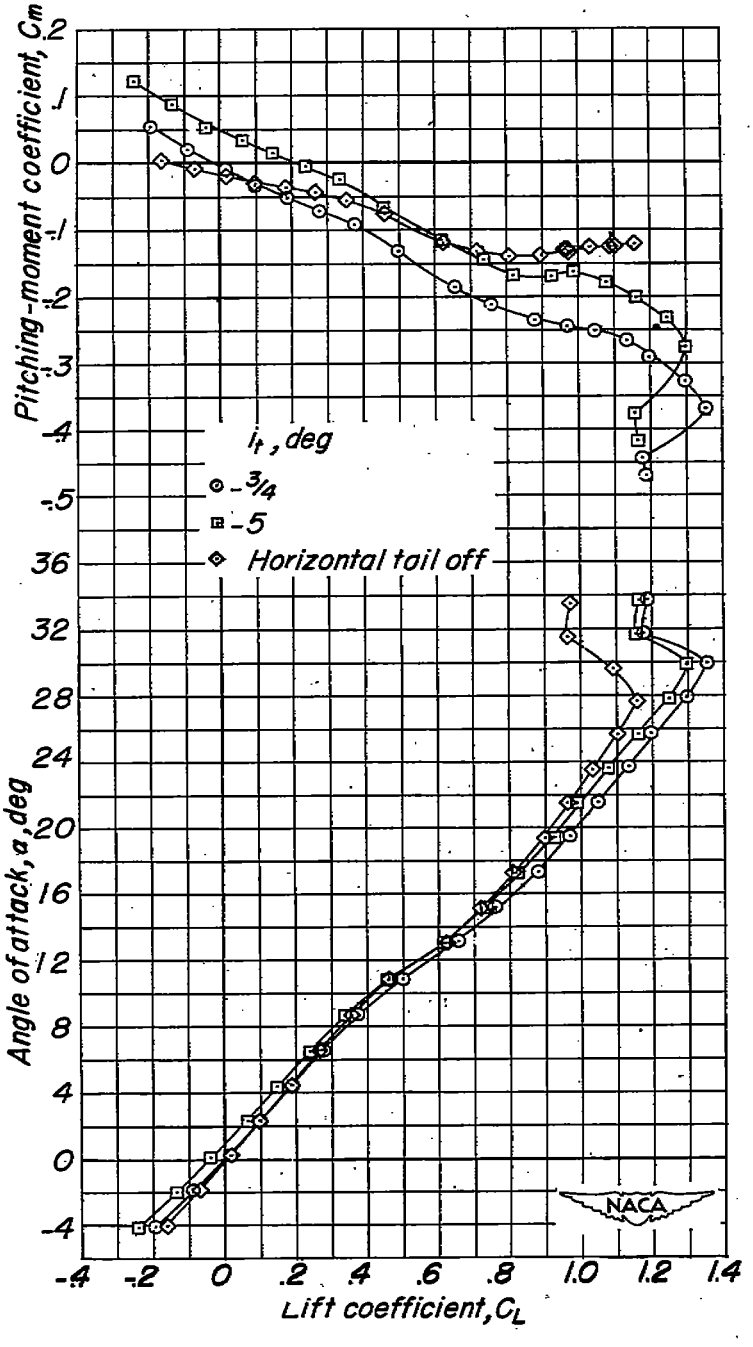

(d) $\Lambda = 60°$.

Figure 8.- Continued.

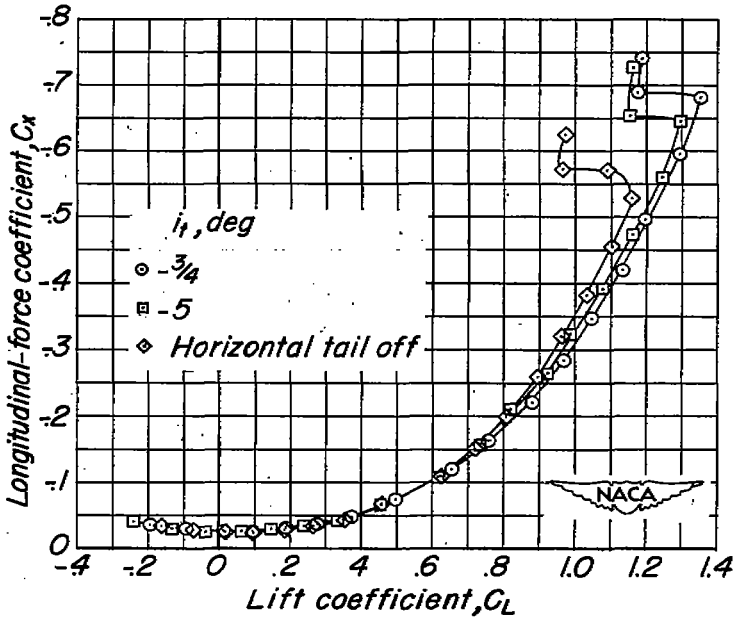

(d) Concluded.

Figure 8.- Concluded.

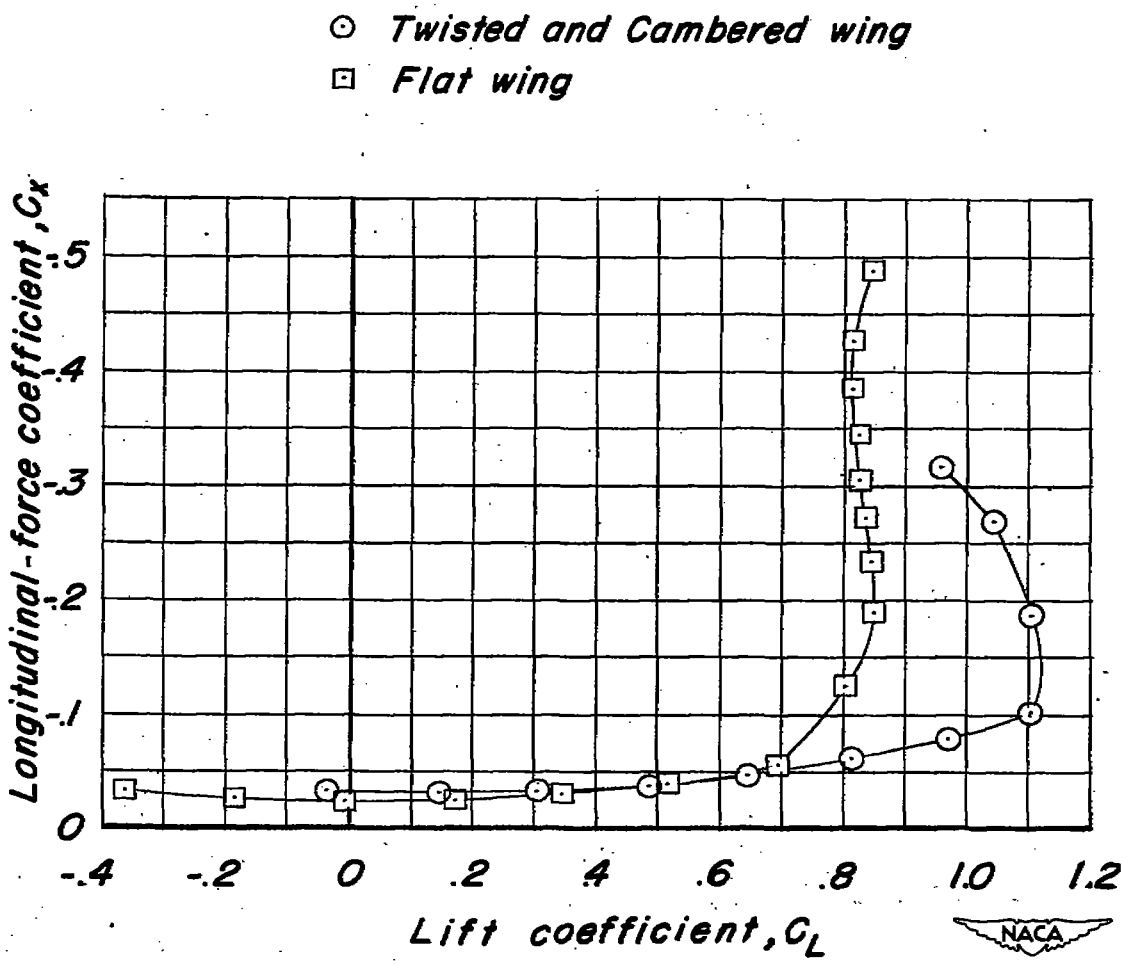

(a) $\Lambda = 20^\circ$.

Figure 9.- The effect of twist and camber on the drag characteristics of the wing-fuselage combination. $\delta_f = 0^\circ$.

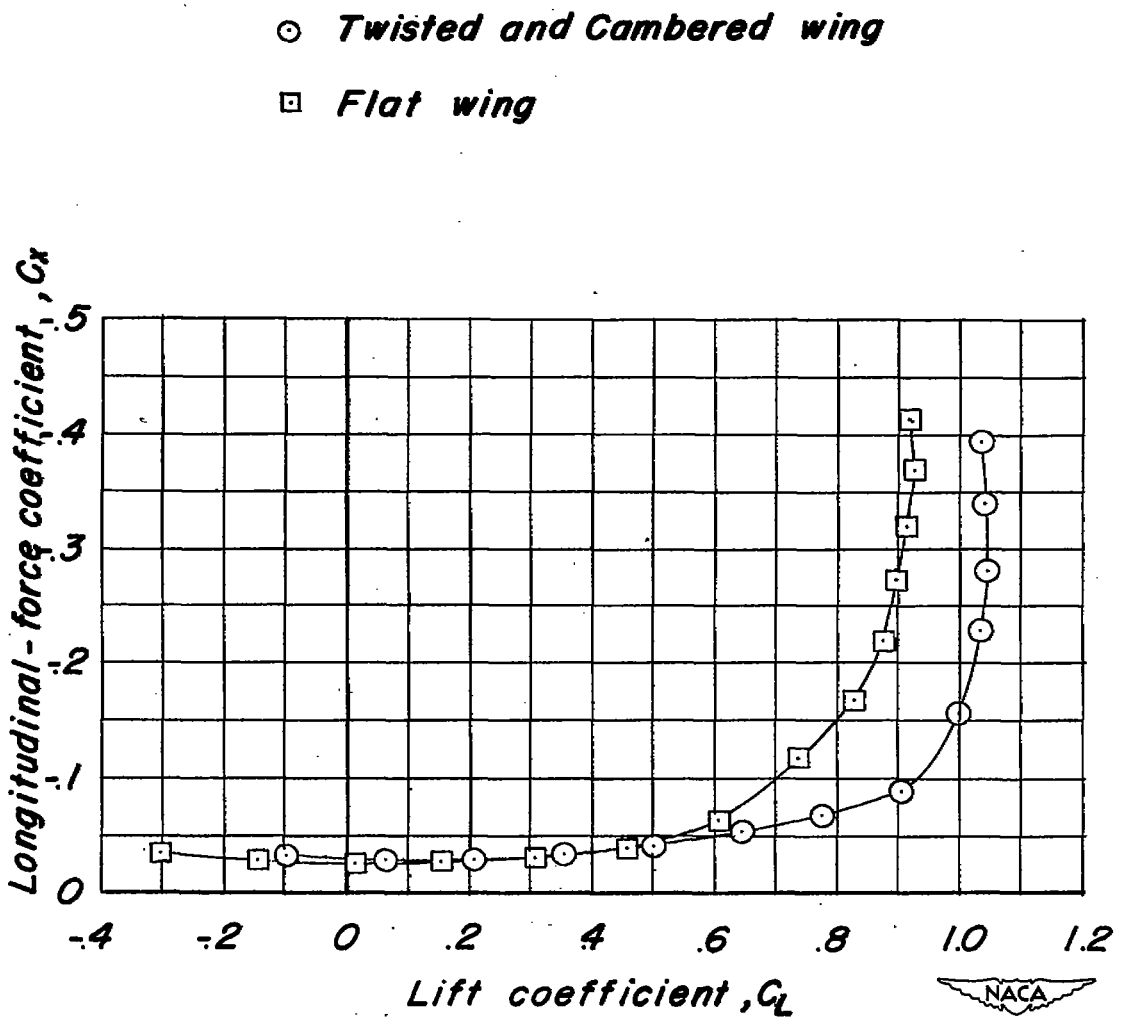

(b) $\Lambda = 35^\circ$.

Figure 9.- Continued.

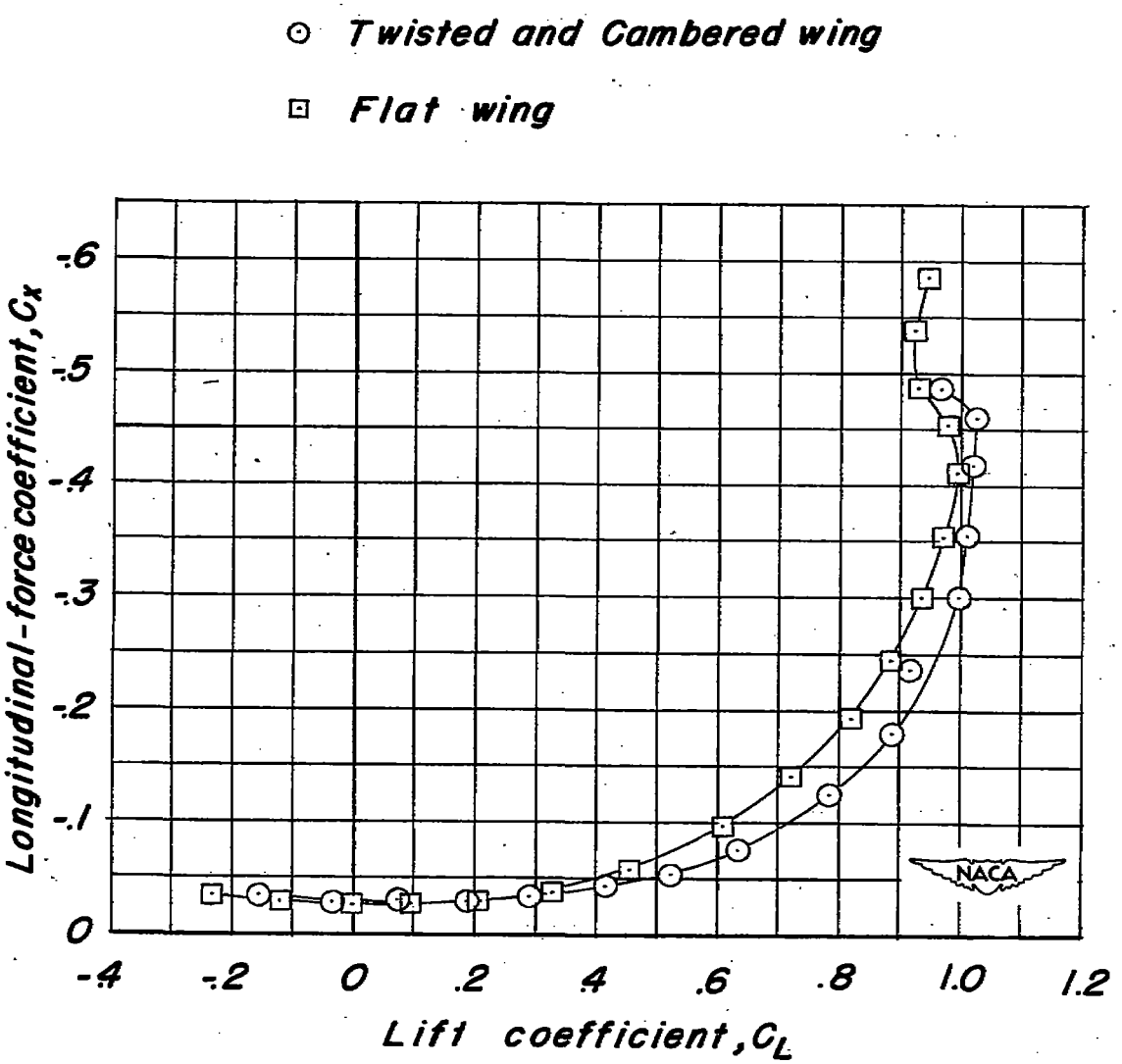

(c) $\Lambda = 50^\circ$.

Figure 9.- Continued.

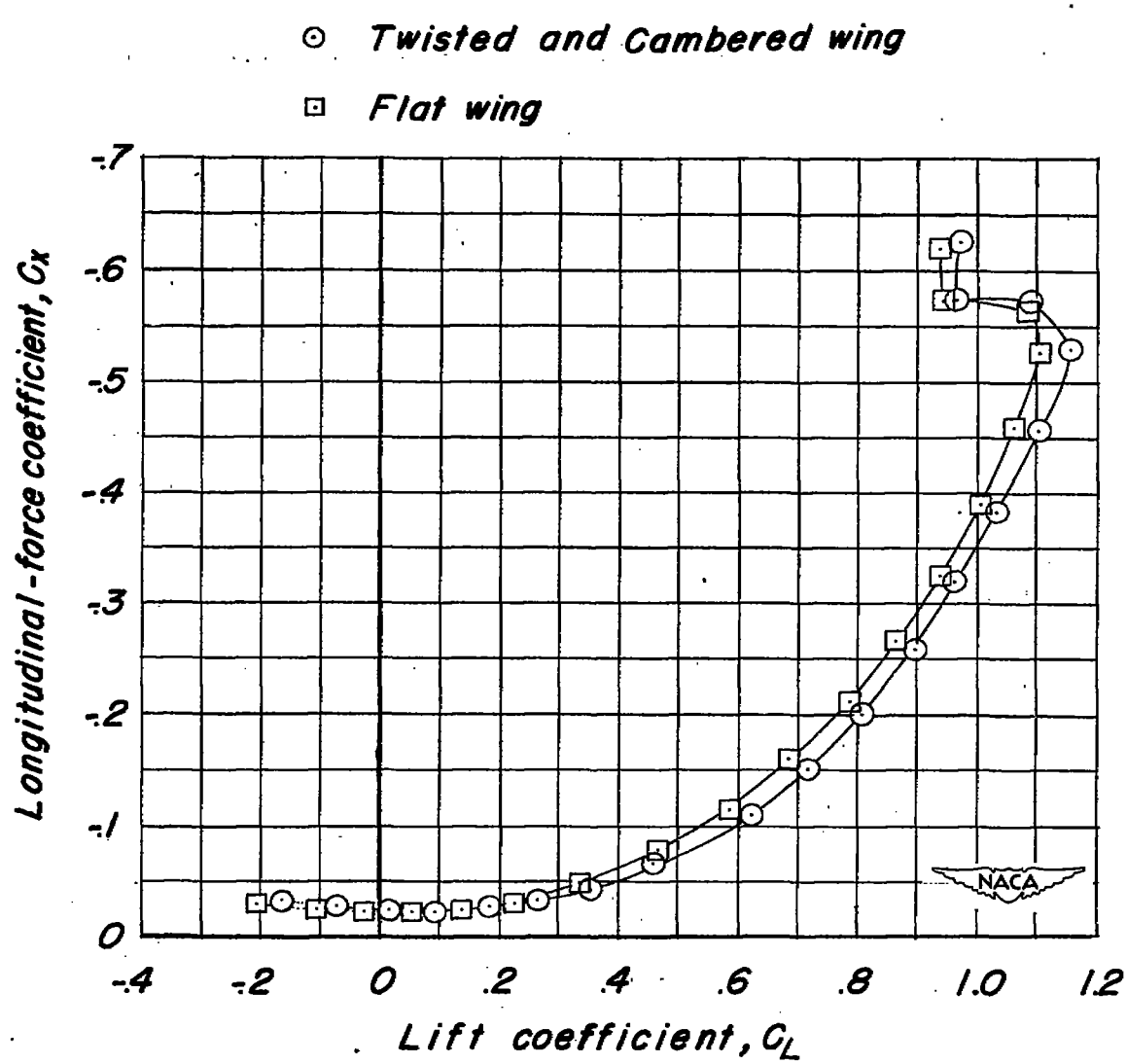

(d) $\Lambda = 60°$.

Figure 9.- Concluded.

[redacted]

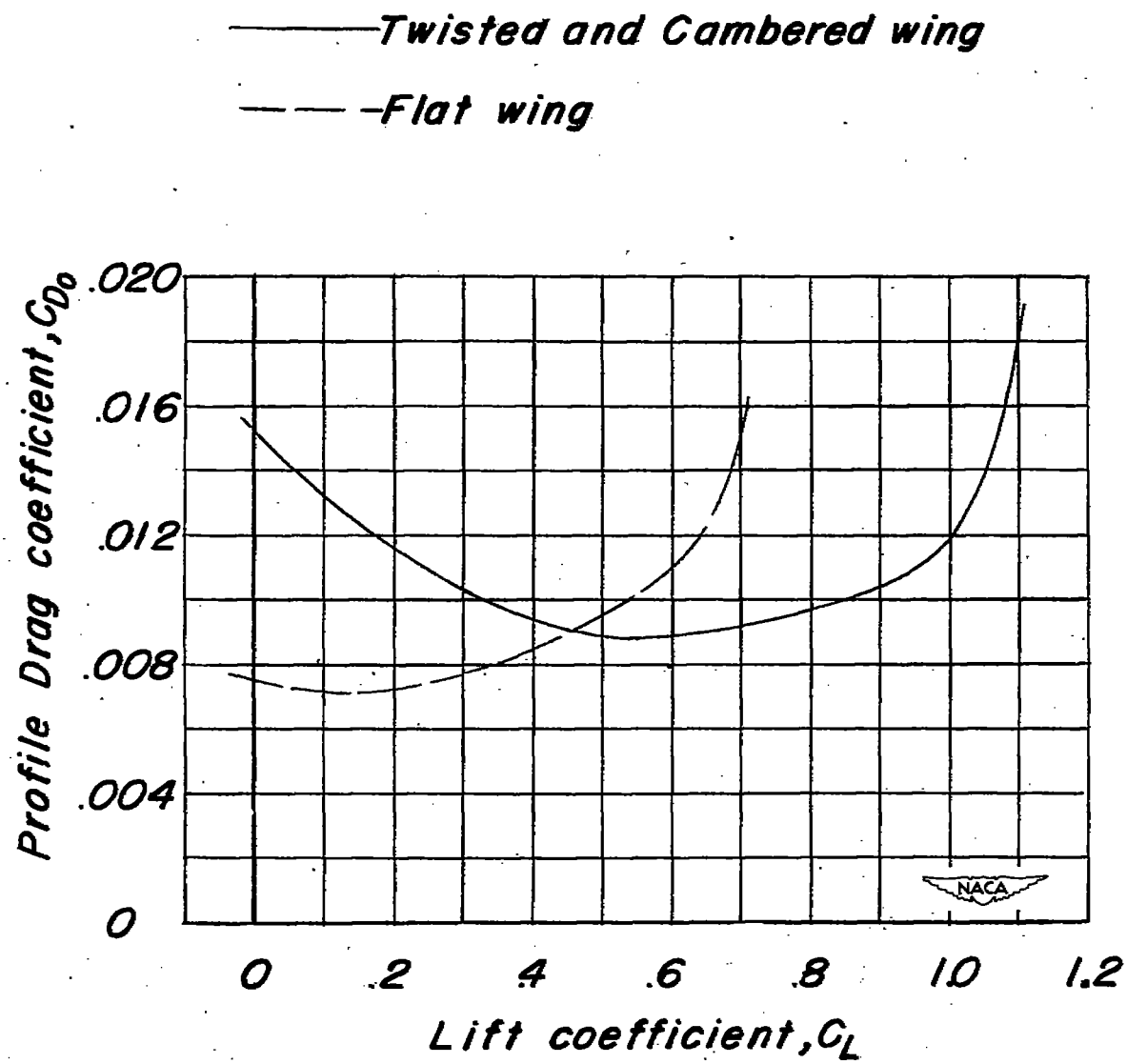

(a) $\Lambda = 20^\circ$.

Figure 10.- The effect of twist and camber on the wing profile-drag characteristics. $\delta_f = 0^\circ$.

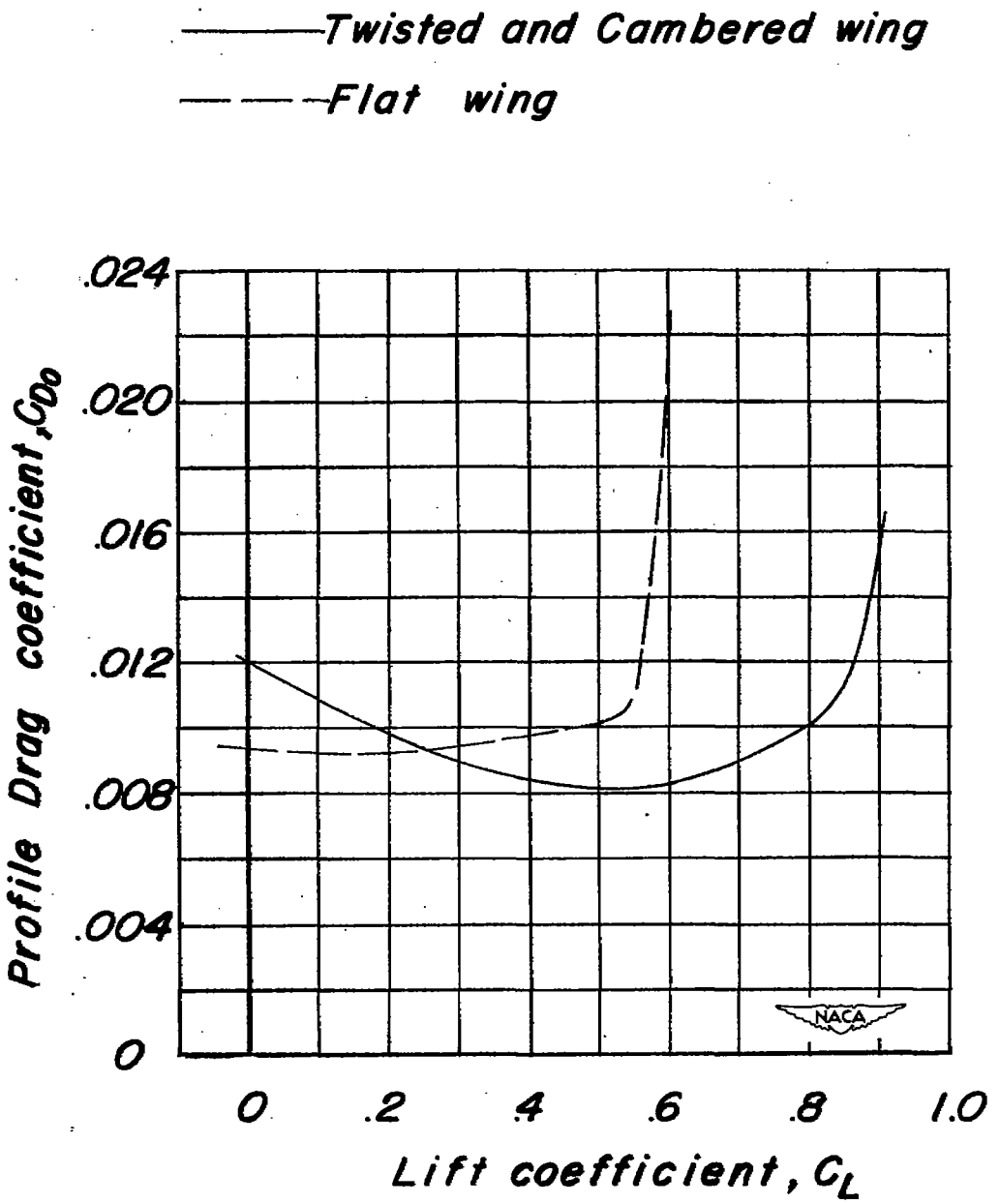

(b) $\Lambda = 35^{\circ}$.

Figure 10.- Continued.

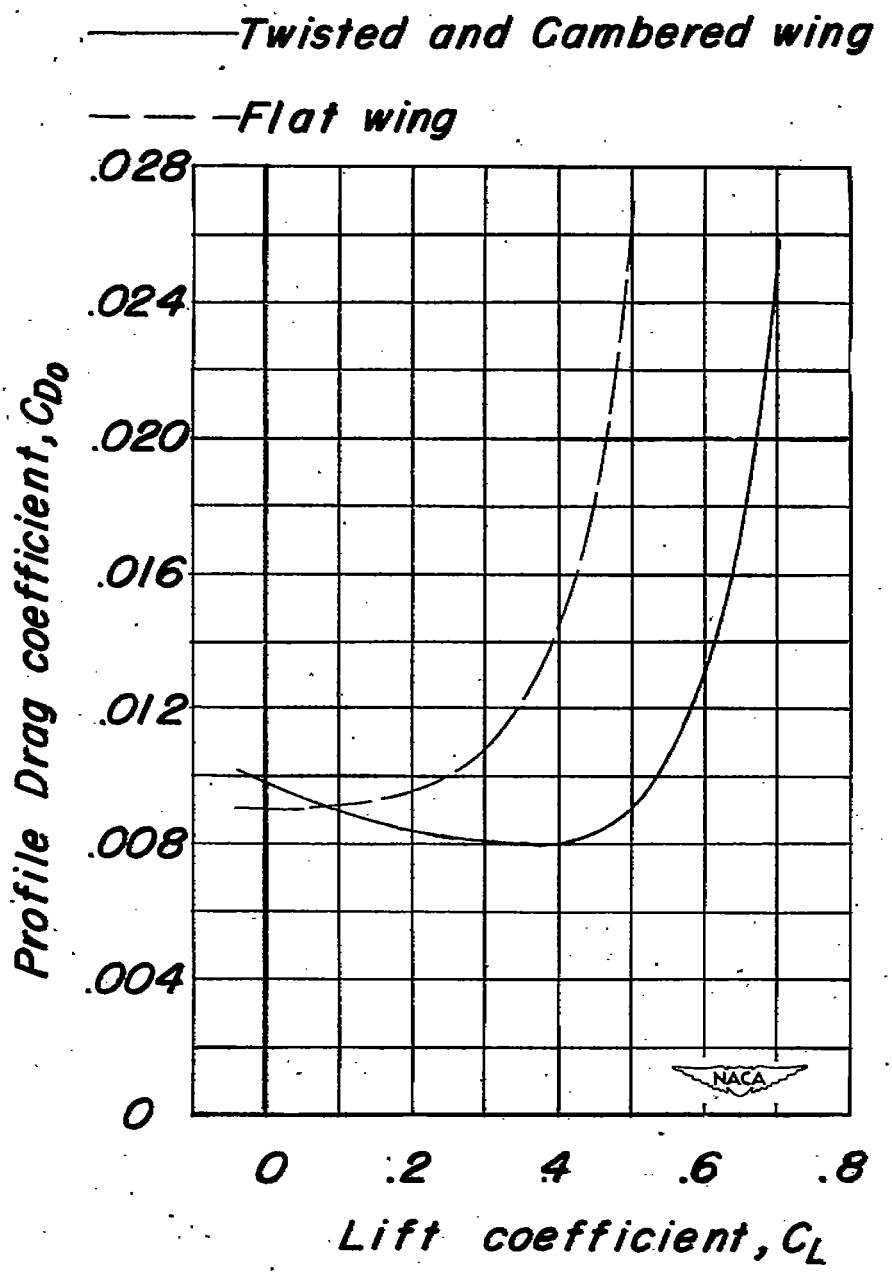

(c) $\Lambda = 50^\circ$.

Figure 10.- Continued.

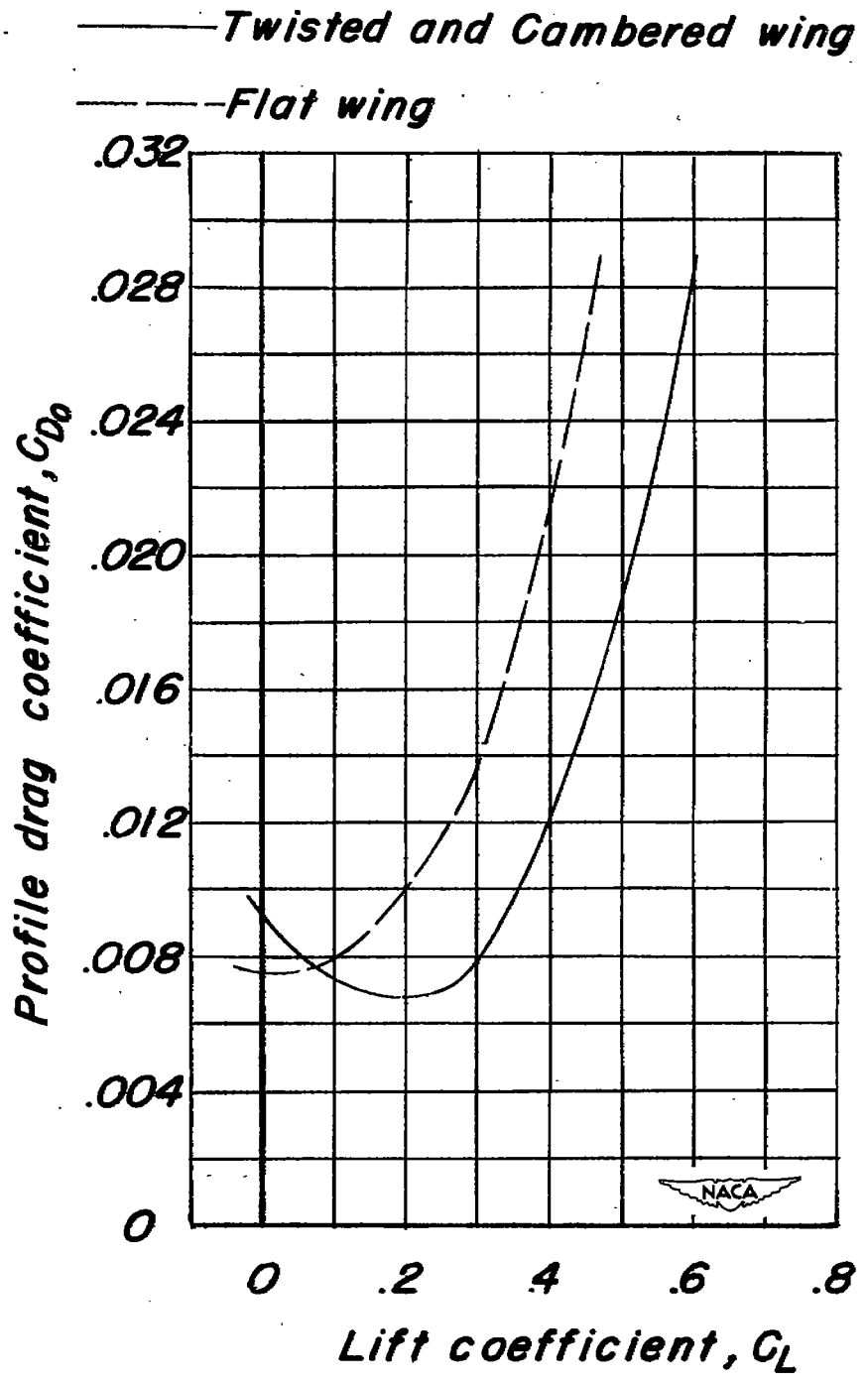

(d) $\Lambda = 60^\circ$.

Figure 10.- Concluded.

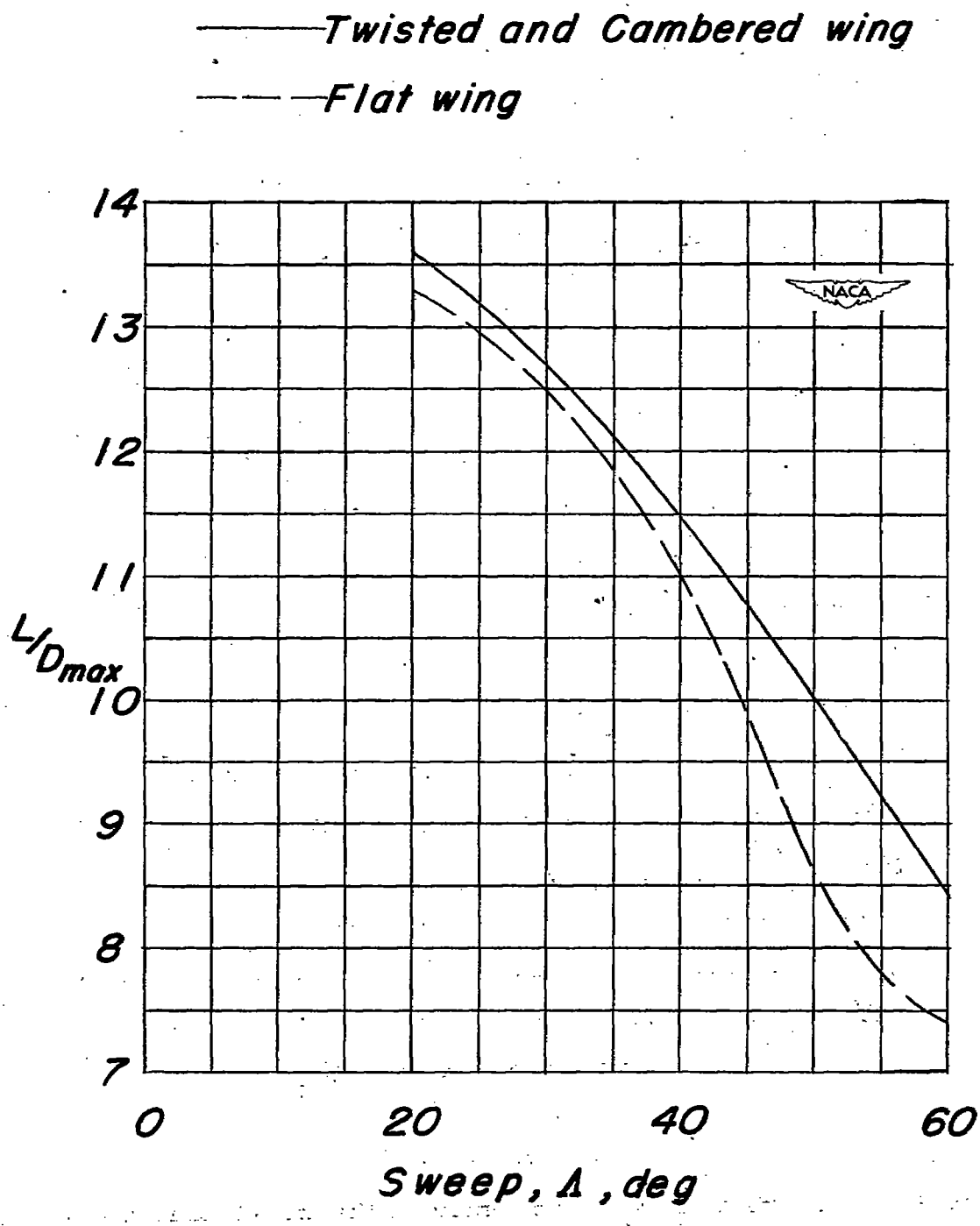

Figure 11.- The effect of twist and camber on the maximum lift-drag ratios of the wing-fuselage combination. $\delta_f = 0^\circ$.

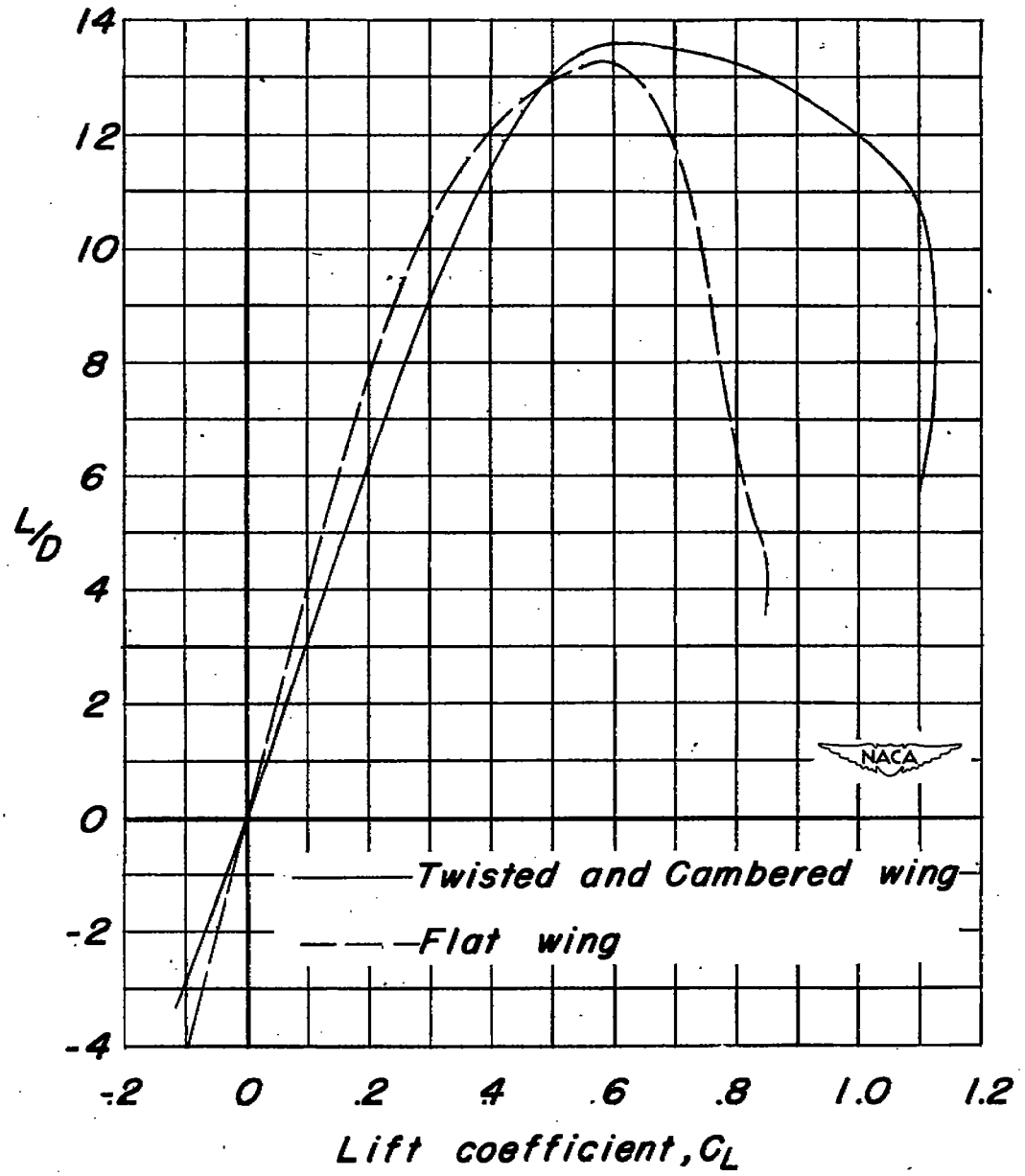

(a) $\Lambda = 20^{\circ}$.

Figure 12.- The effect of twist and camber on the lift-drag ratios of the wing-fuselage combination. $\delta_f = 0^{\circ}$.

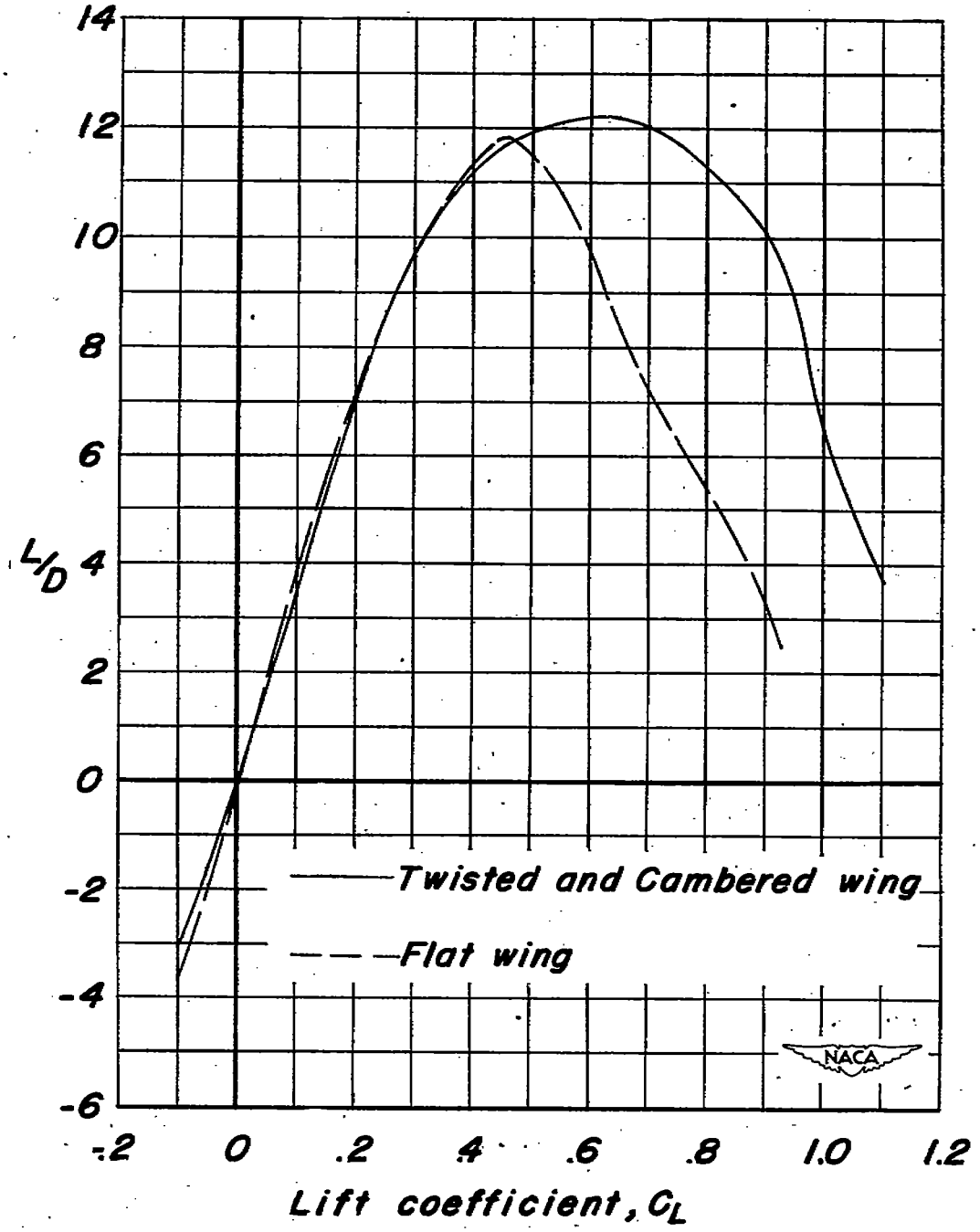

(b) $\Lambda = 35°$.

Figure 12.- Continued.

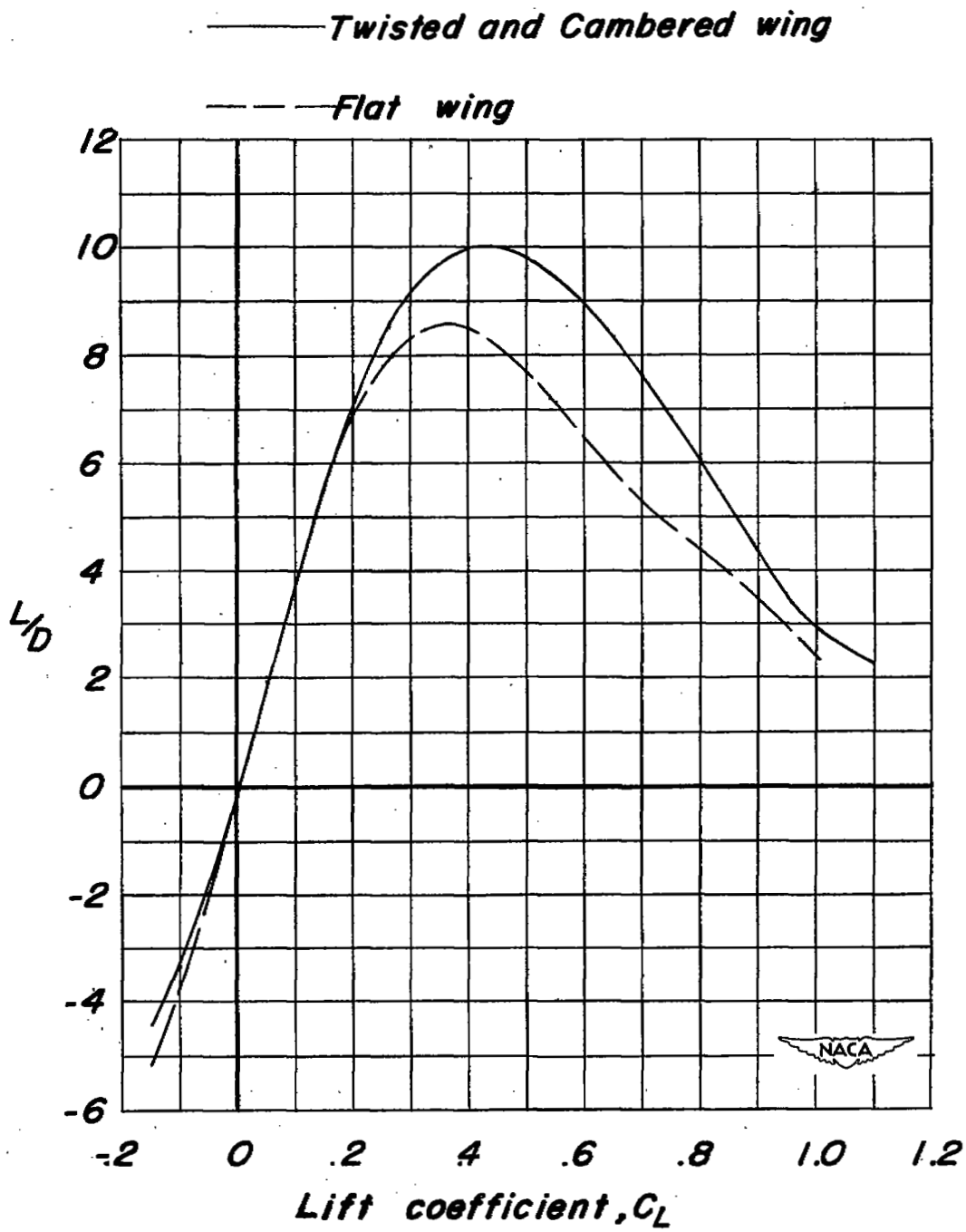

(c) $\Lambda = 50^\circ$.

Figure 12.- Continued.

[redacted]

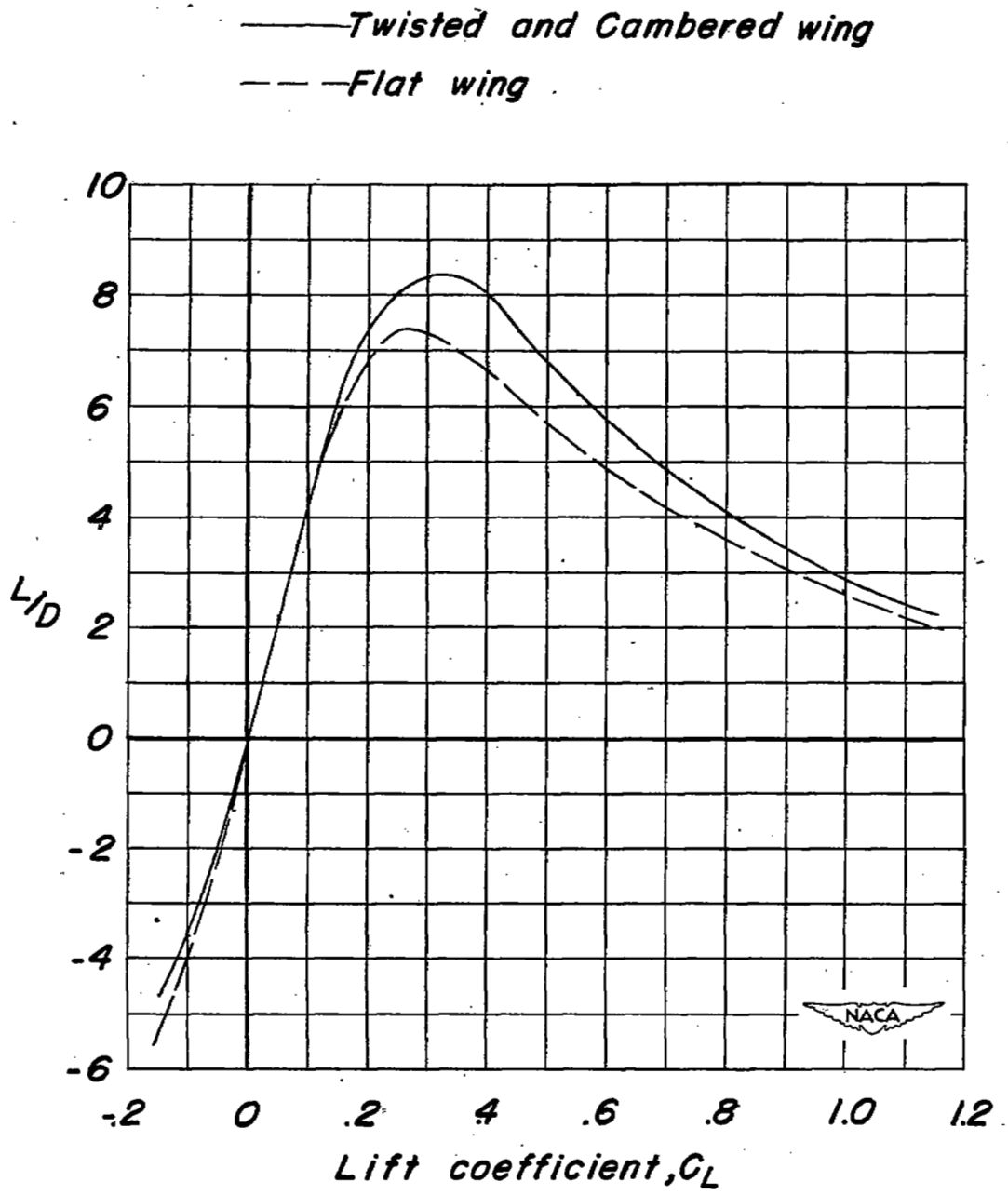

(d) $\Lambda = 60^\circ$.

Figure 12.- Concluded.

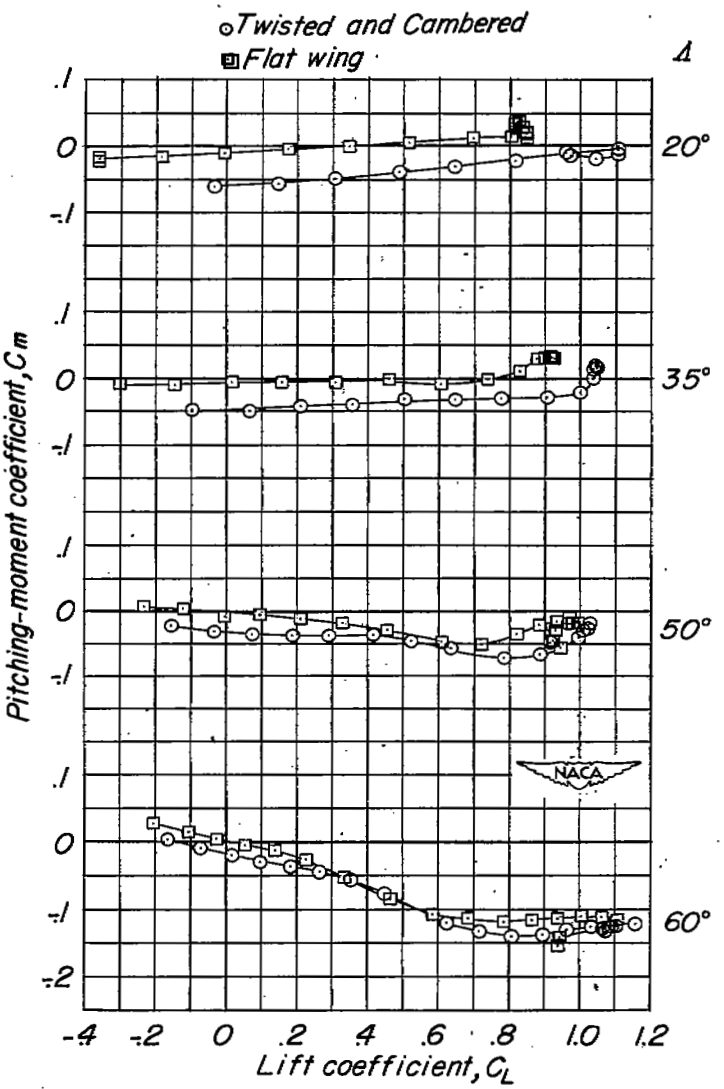

Figure 13.- The effect of twist and camber on the tail-off pitching-moment of the test model. $\delta_f = 0°$.

[redacted]

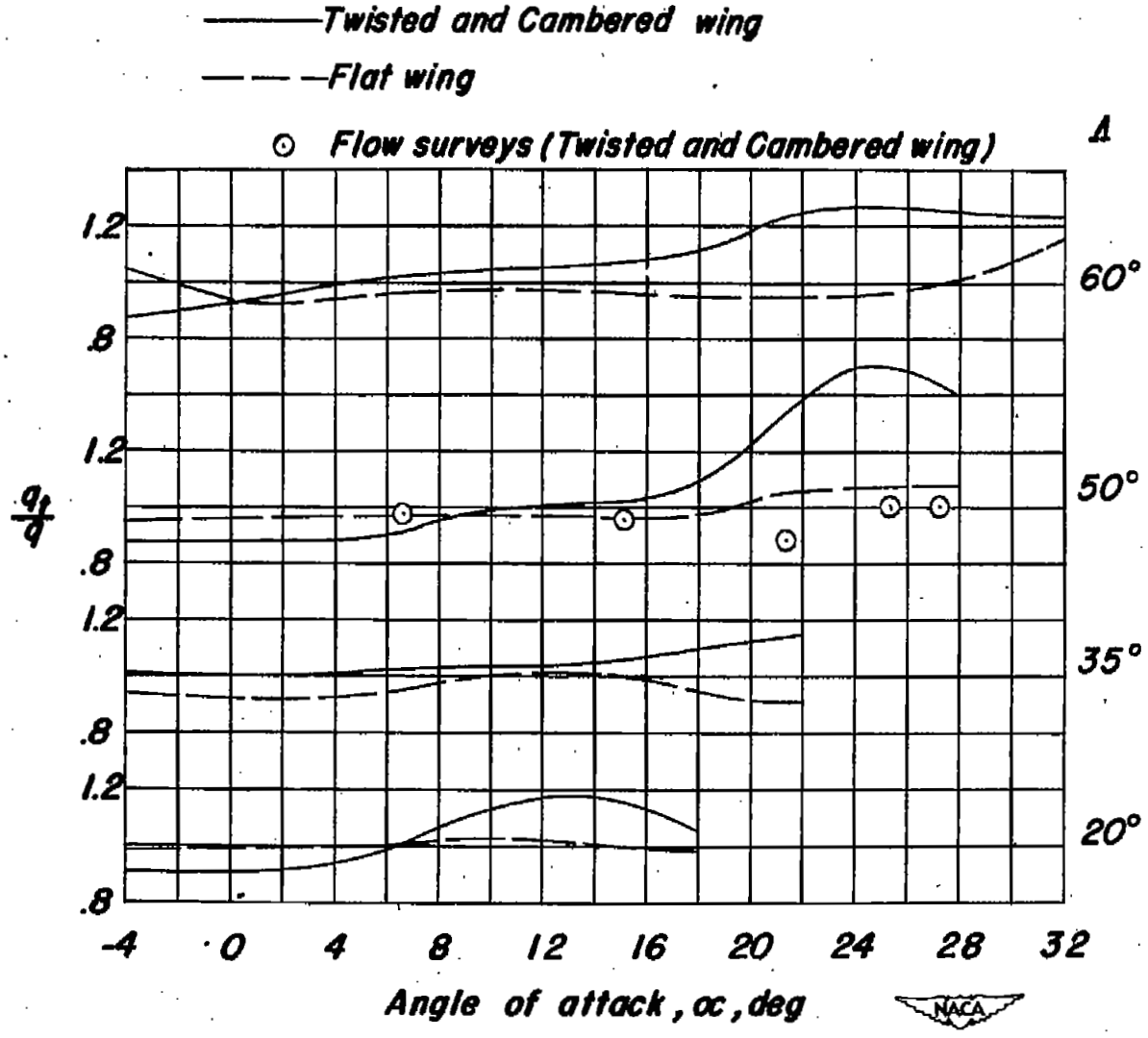

Figure 14.- The effect of twist and camber on the dynamic pressure at the tail of the test model. $\delta_f = 0^\circ$.

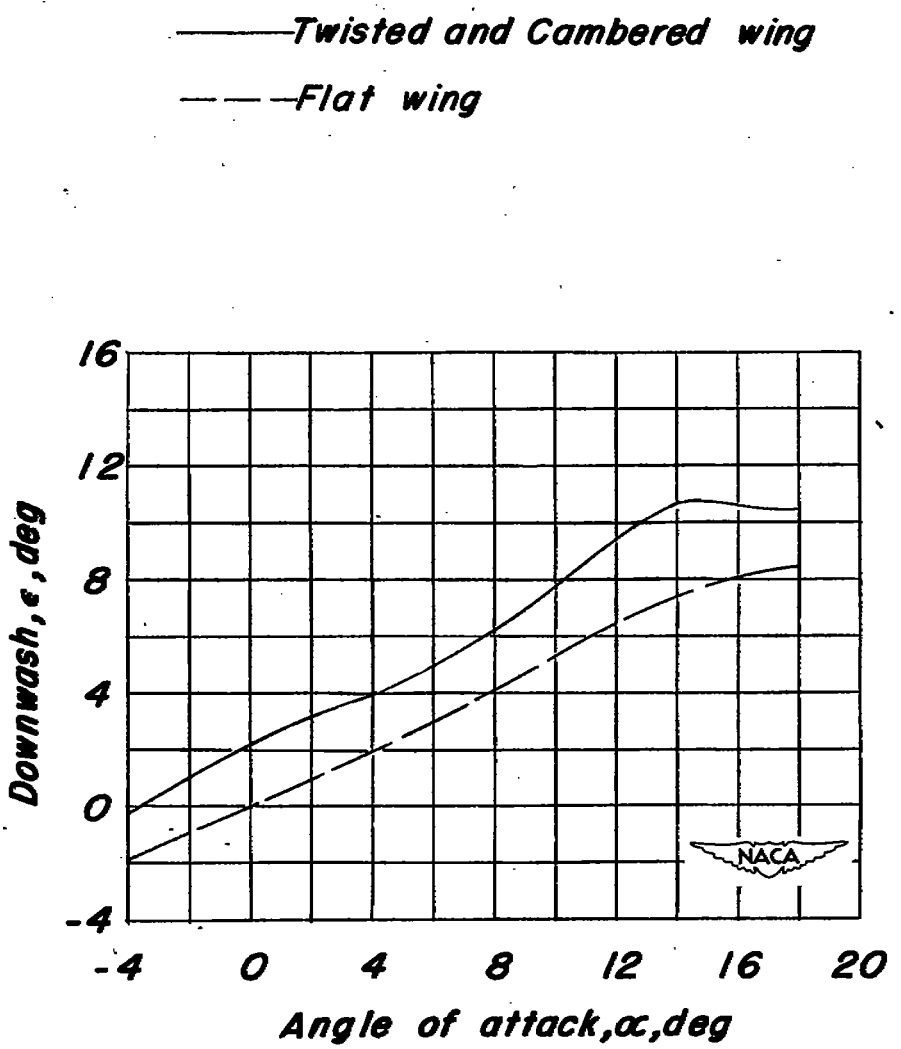

(a) $\Lambda = 20^{\circ}$.

Figure 15.- The effect of twist and camber on the downwash at the tail of the test model. $\delta_f = 0^{\circ}$.

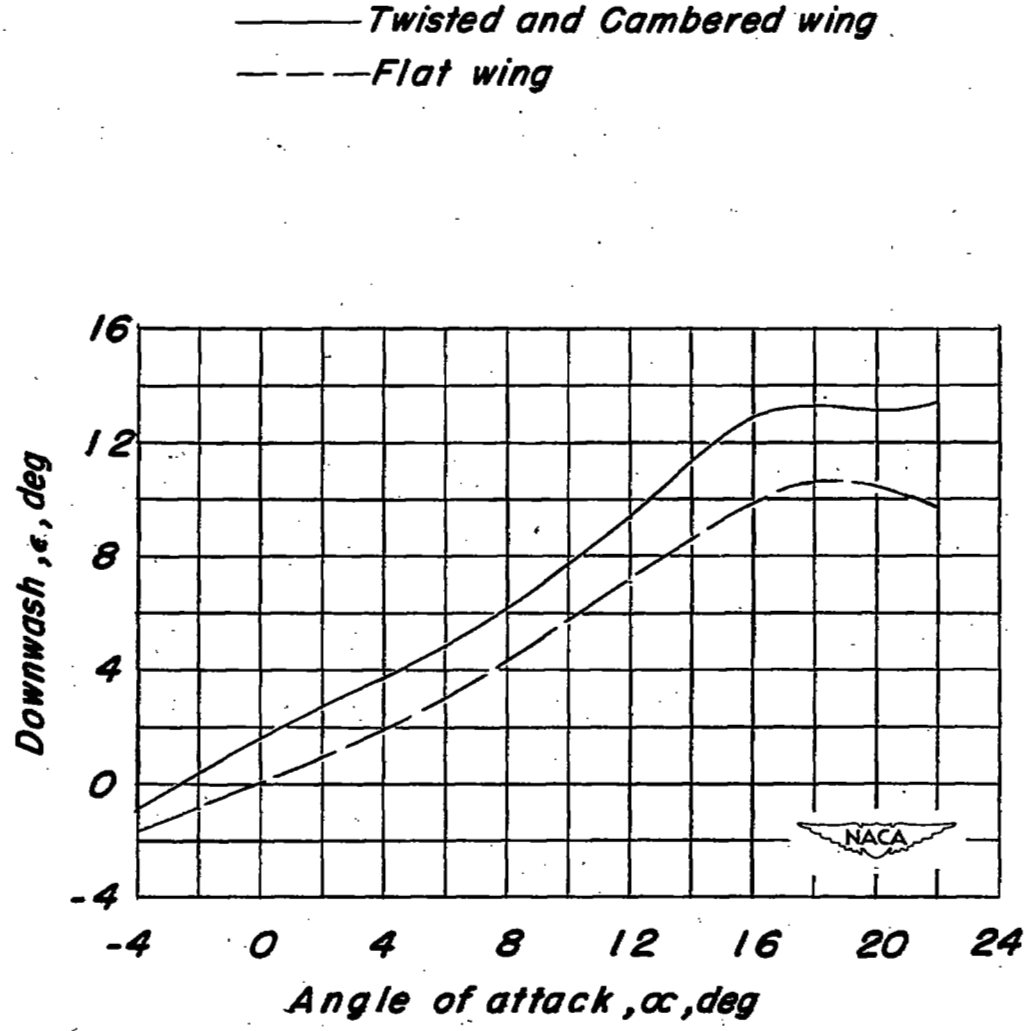

(b) $\Lambda = 35^{\circ}$.

Figure 15.- Continued.

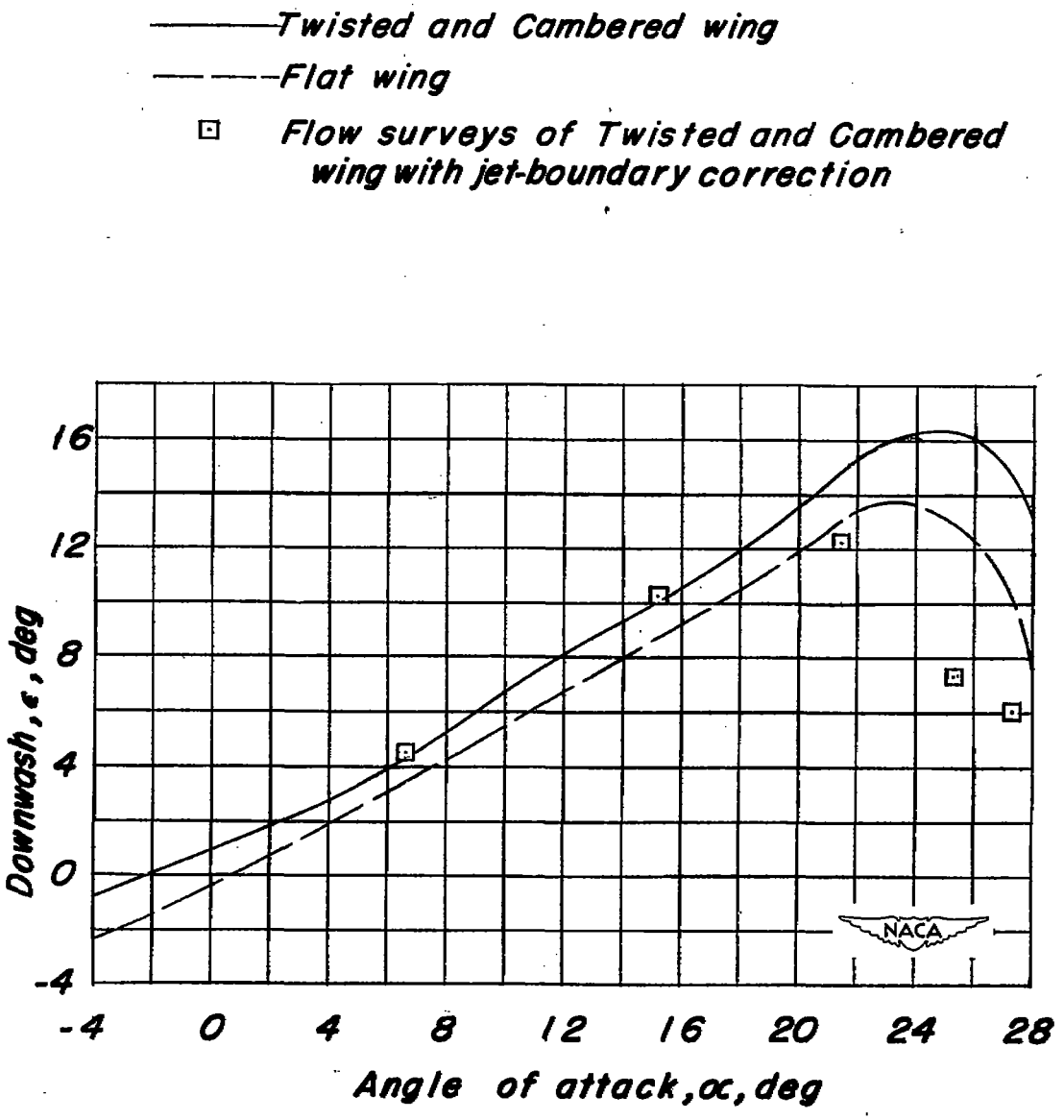

(c) $\Lambda = 50^{\circ}$.

Figure 15.- Continued.

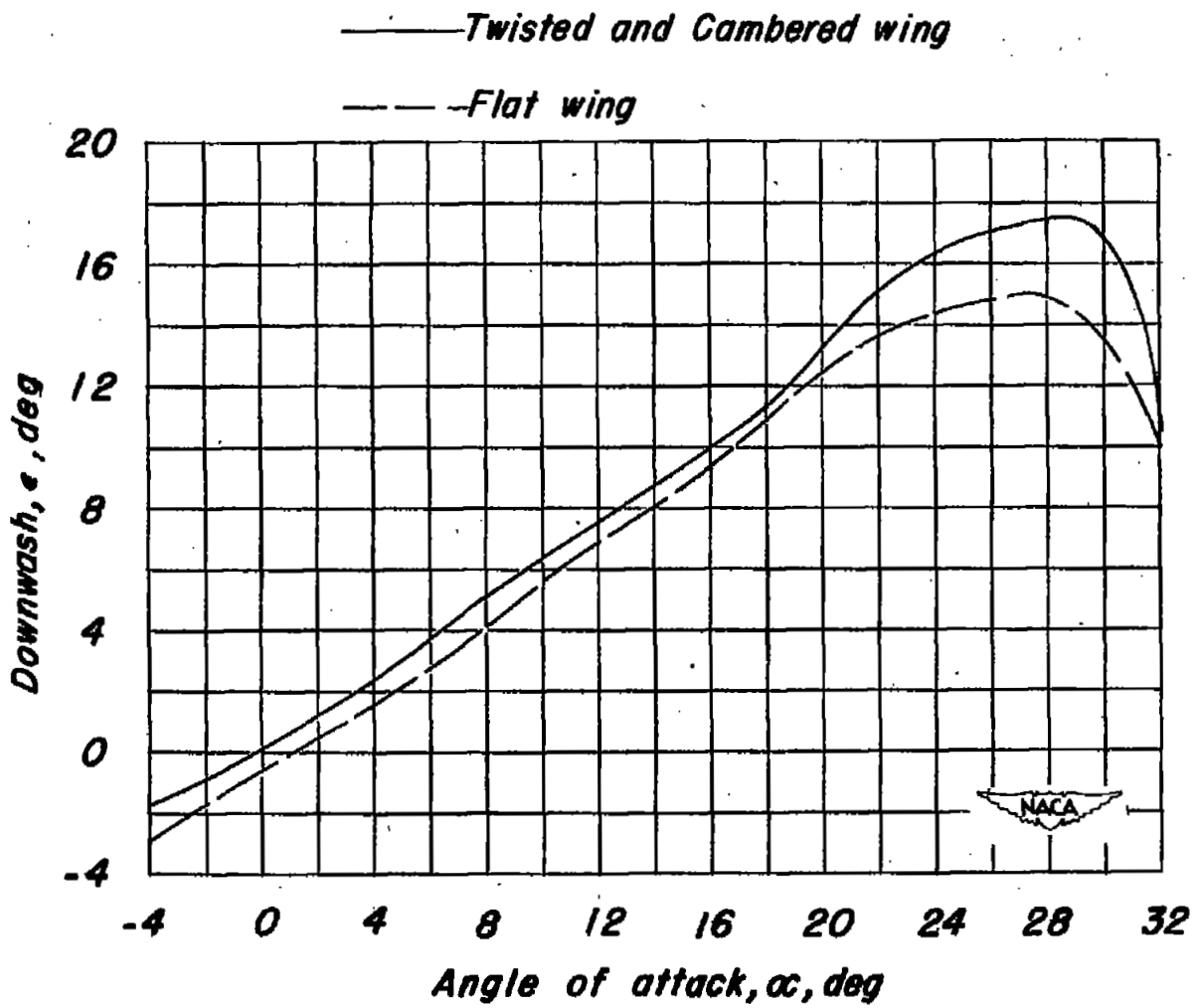

(d) $\Lambda = 60°$.

Figure 15.- Concluded.

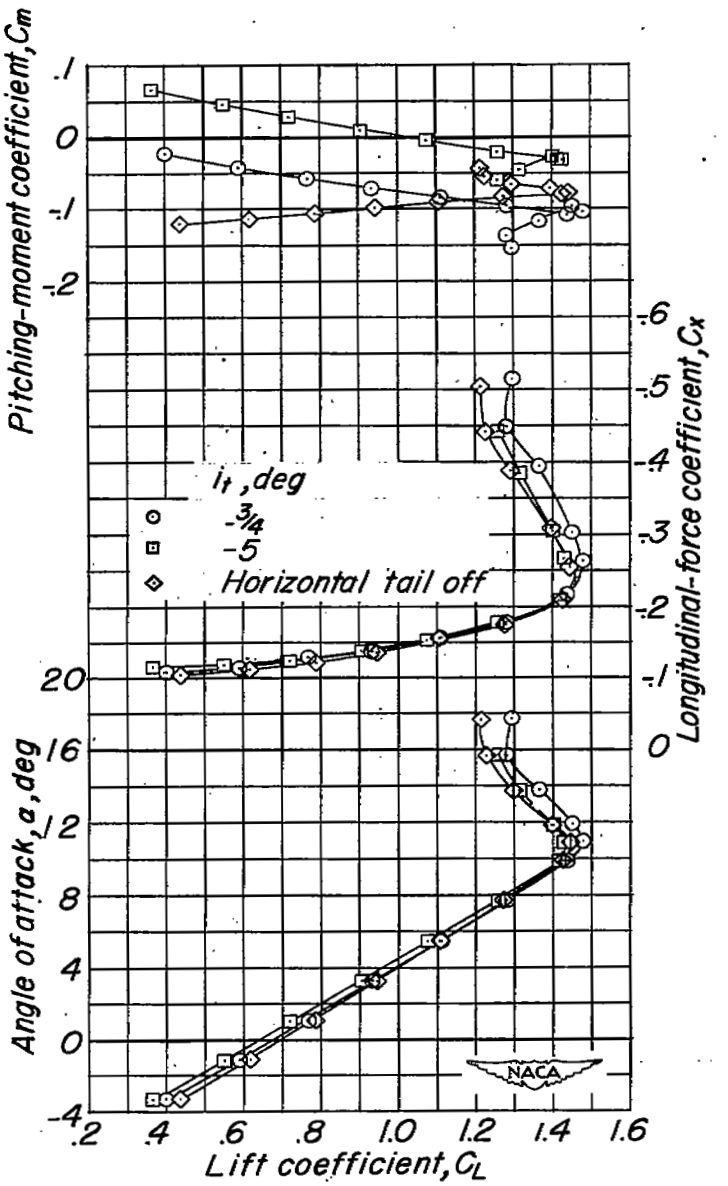

(a) $\Lambda = 20^\circ$.

Figure 16.- The longitudinal aerodynamic characteristics of the twisted and cambered wing model. $\delta_f = 50^\circ$.

[redacted]

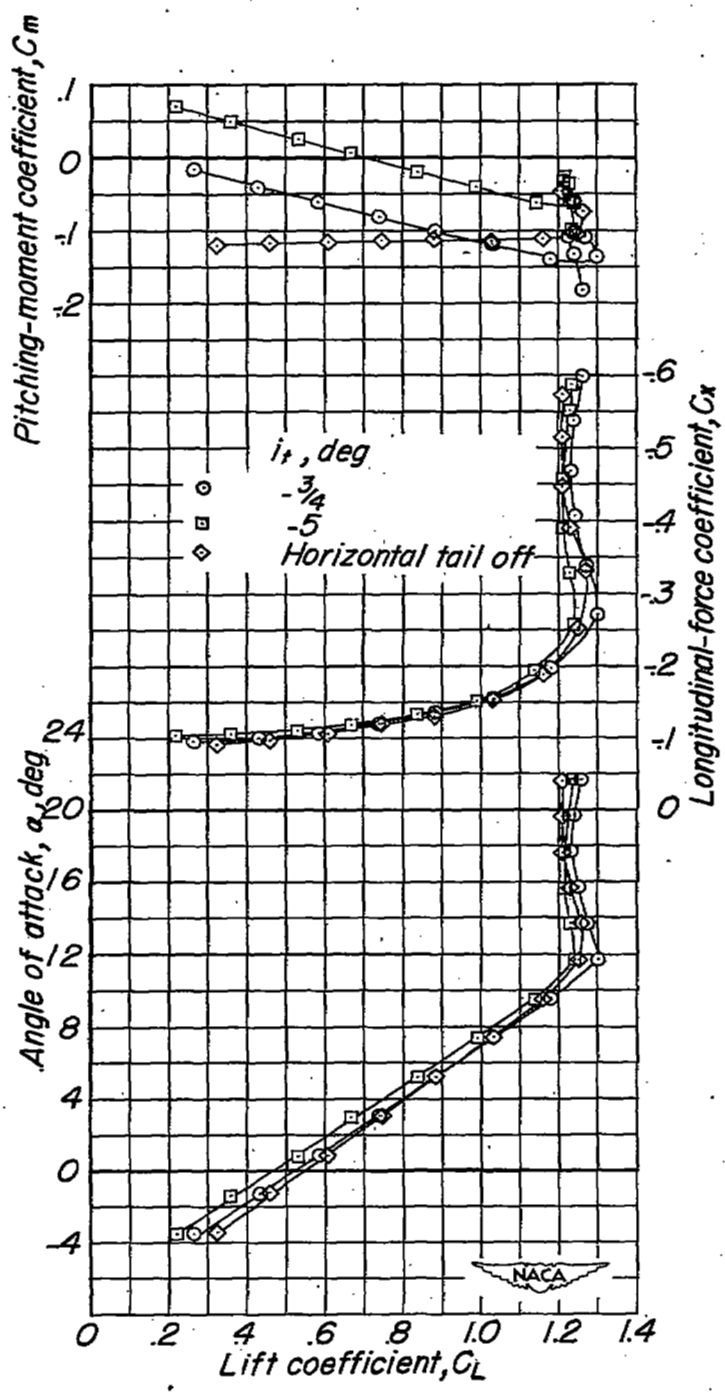

(b) $\Lambda = 35^\circ$.

Figure 16.- Continued.

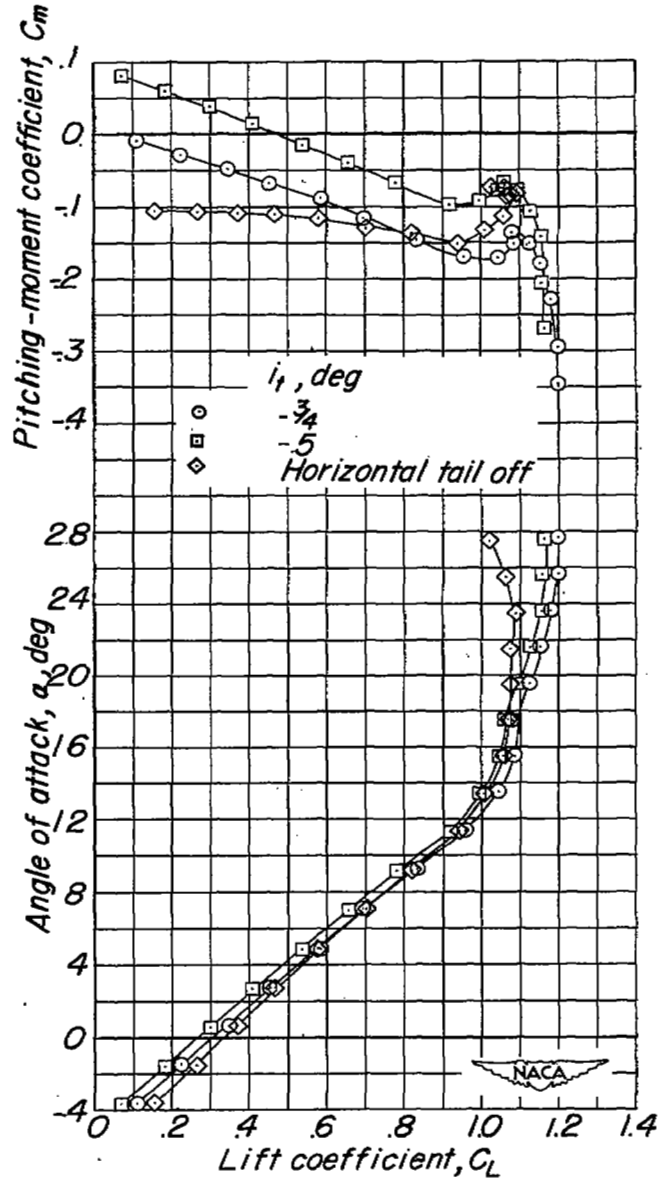

(c) $\Lambda = 50°$.

Figure 16.- Continued.

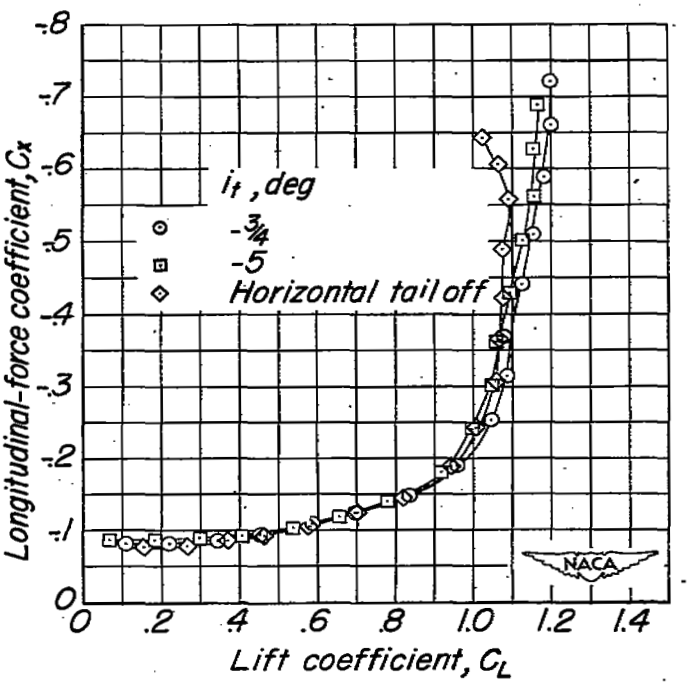

(c) Concluded.

Figure 16.- Concluded.

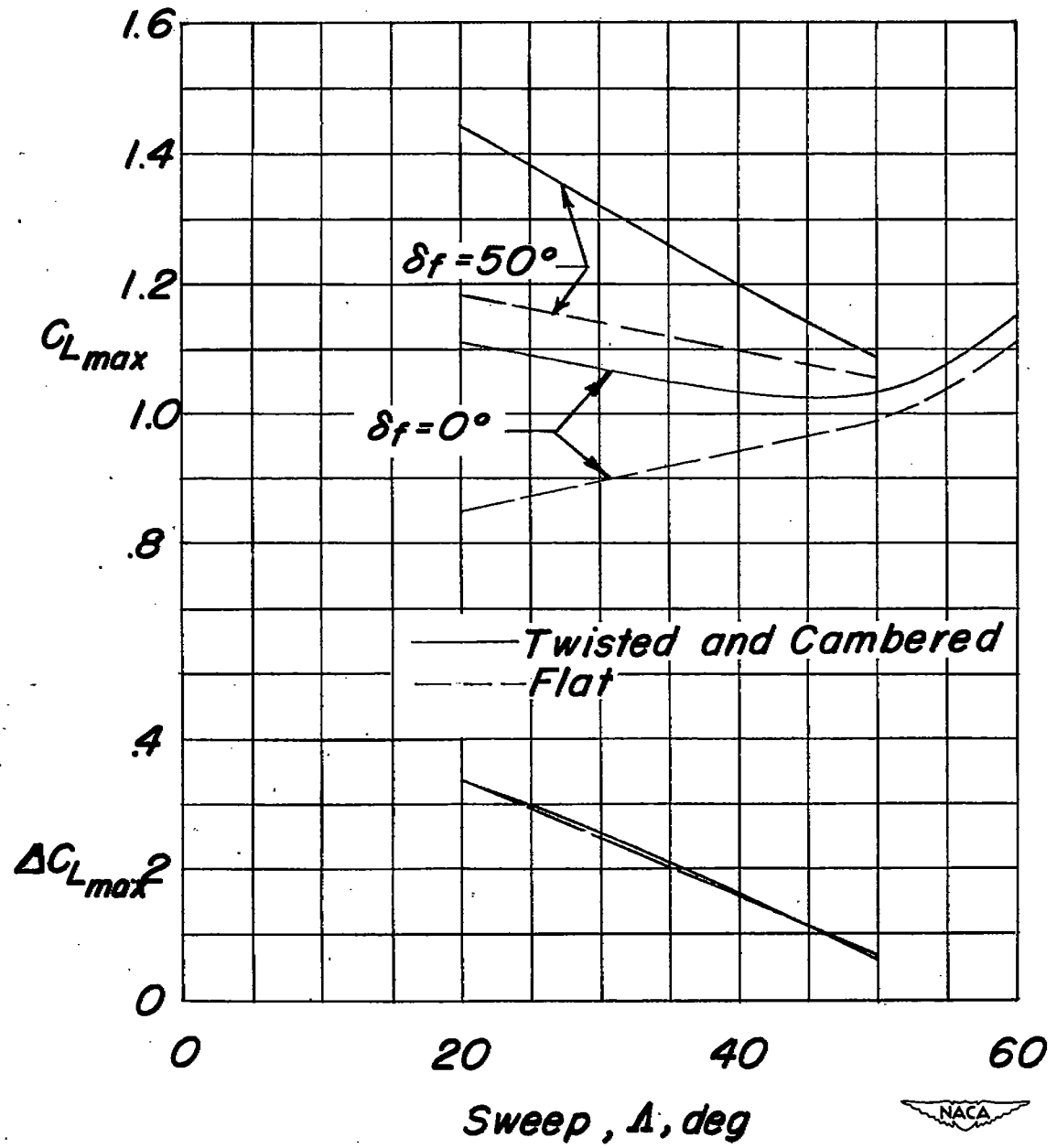

Figure 17.- The effect of twist and camber on the maximum lift coefficient for the wing-fuselage combination.

[redacted]

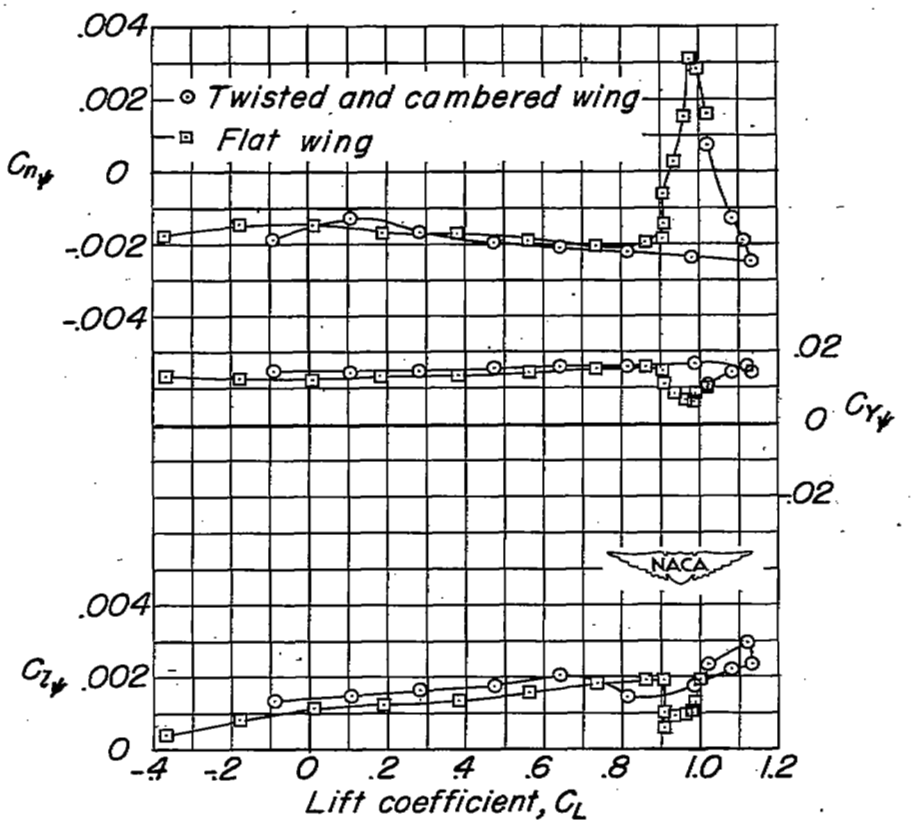

(a) $\Lambda = 20^\circ$.

Figure 18.- The effect of twist and camber on the lateral stability parameters of the test model. $\delta_f = 0^\circ$; $i_t = -\frac{3^\circ}{4}$.

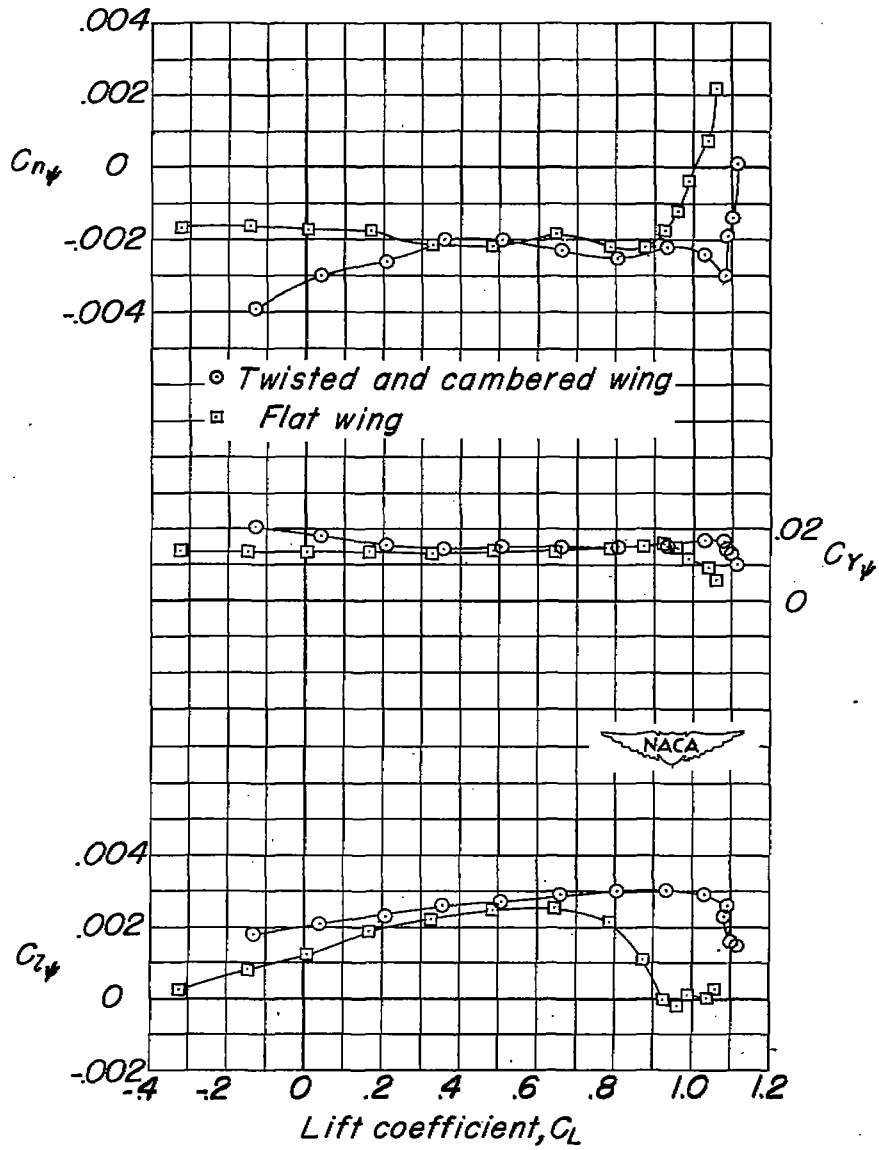

(b) $\Lambda = 35^\circ$.

Figure 18.- Continued.

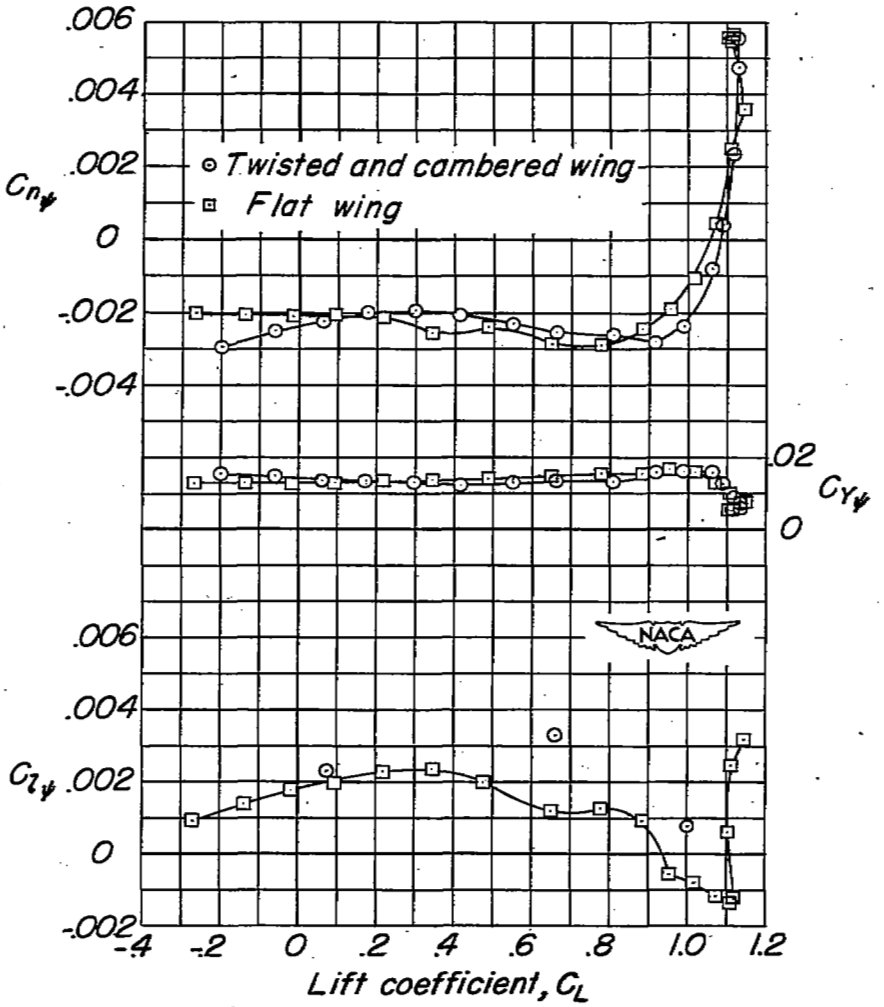

(c) $\Lambda = 50^\circ$.

Figure 18.- Continued.

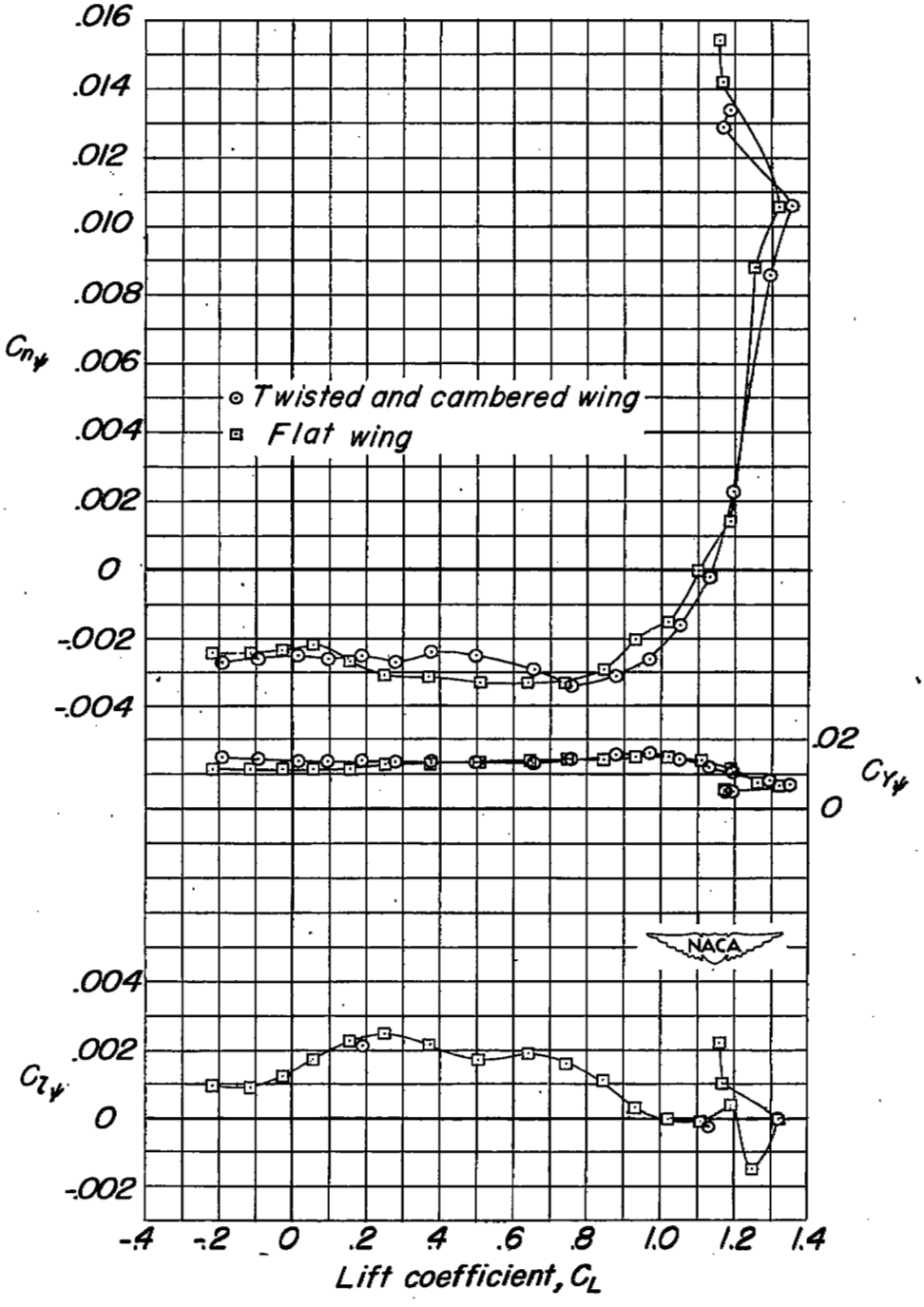

(d) $\Lambda = 60°$.

Figure 18.- Concluded.

[redacted]

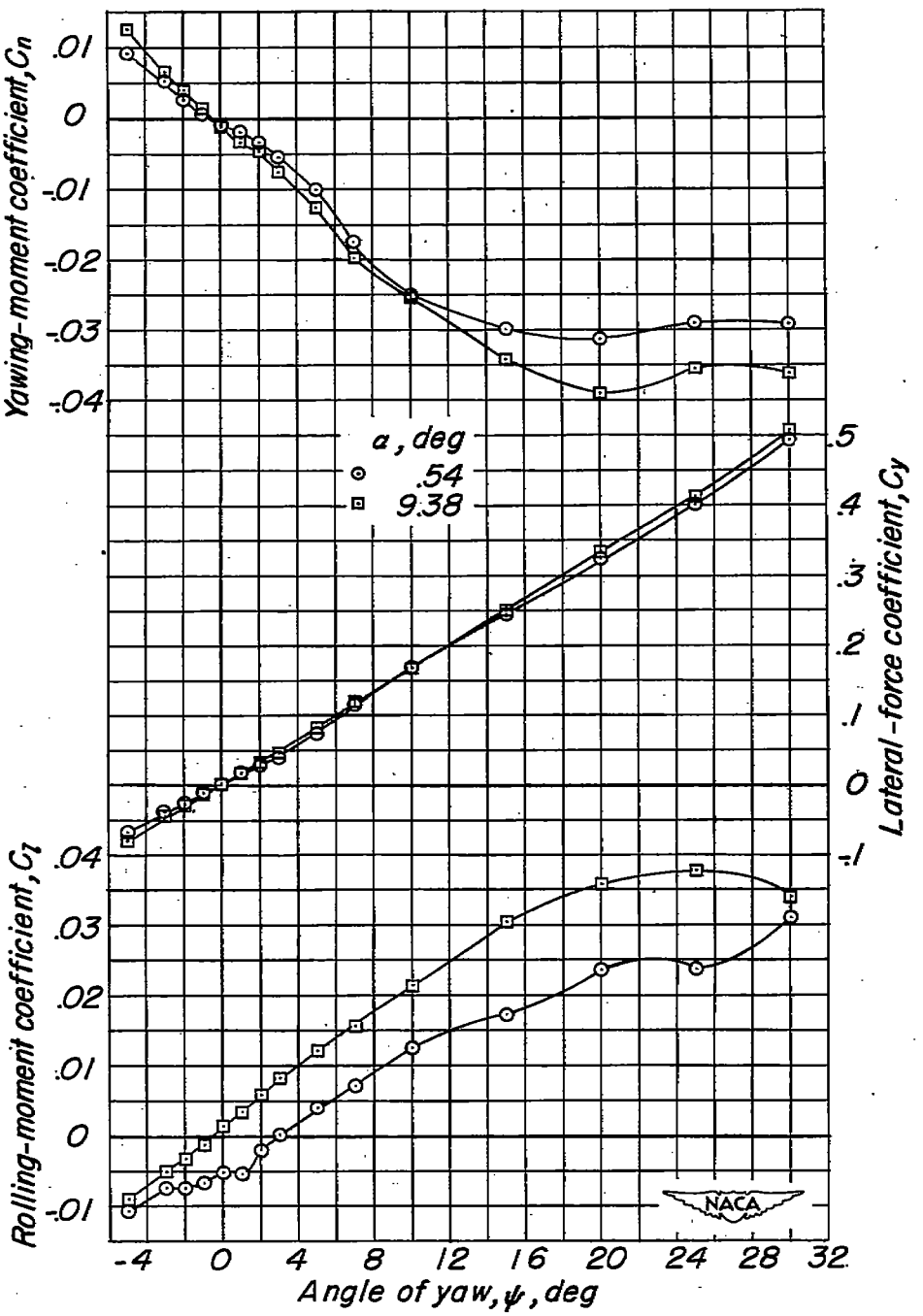

(a) $\Lambda = 20^\circ$.

Figure 19.- The effect of angle of attack on the aerodynamic characteristics in yaw of the twisted and cambered wing model. $\delta_f = 0^\circ$; $i_t = -\frac{3^\circ}{4}$.

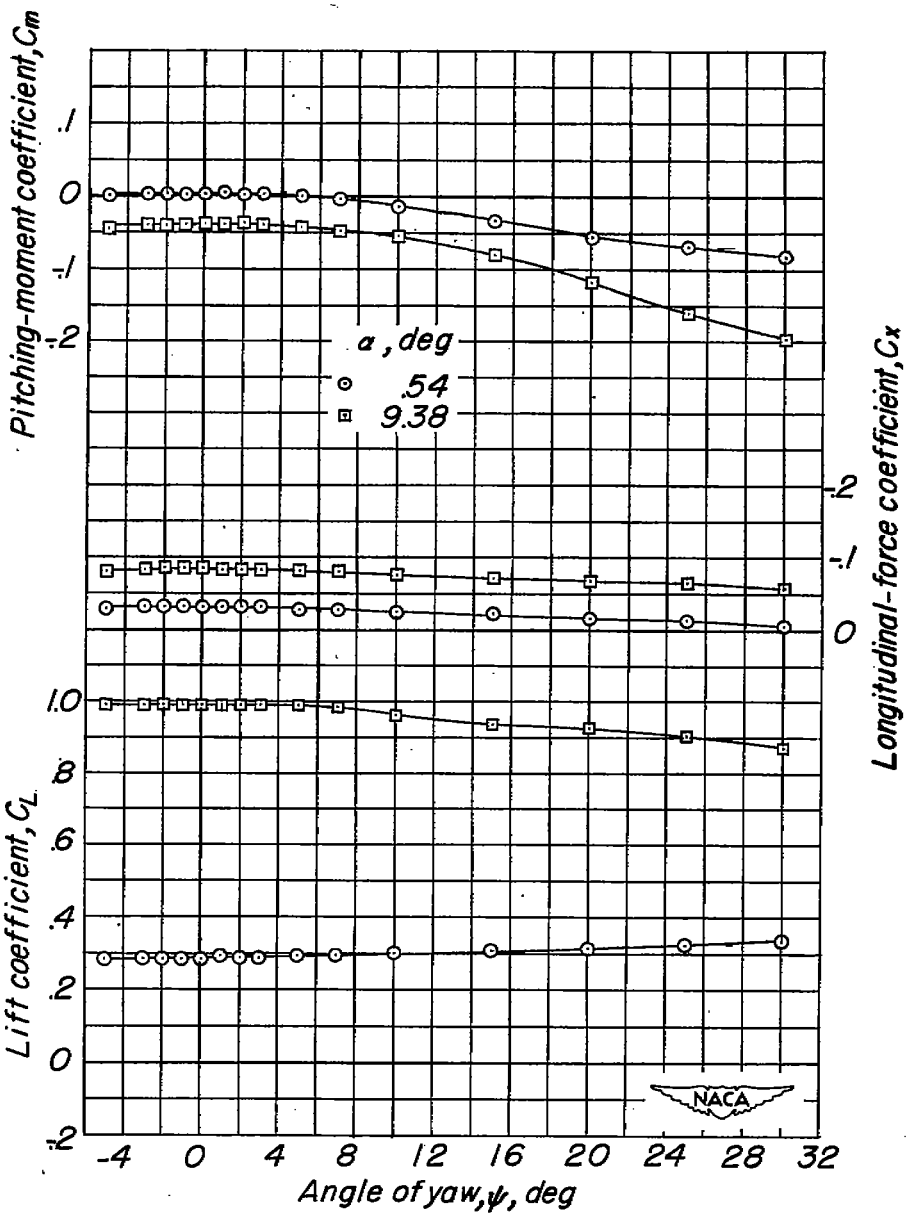

(a) Concluded.

Figure 19.- Continued.

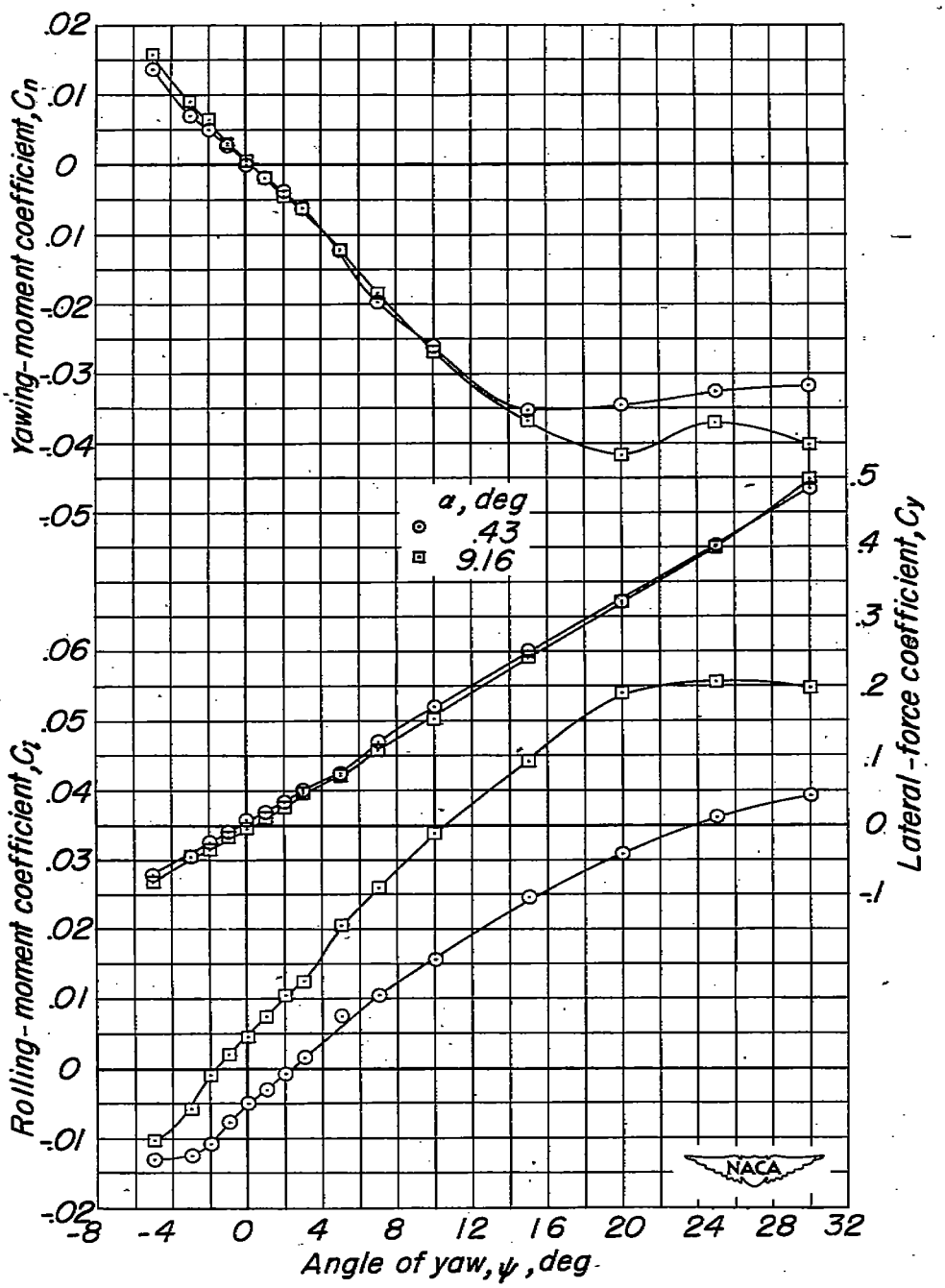

(b) $\Lambda = 35^{\circ}$.

Figure 19.- Continued.

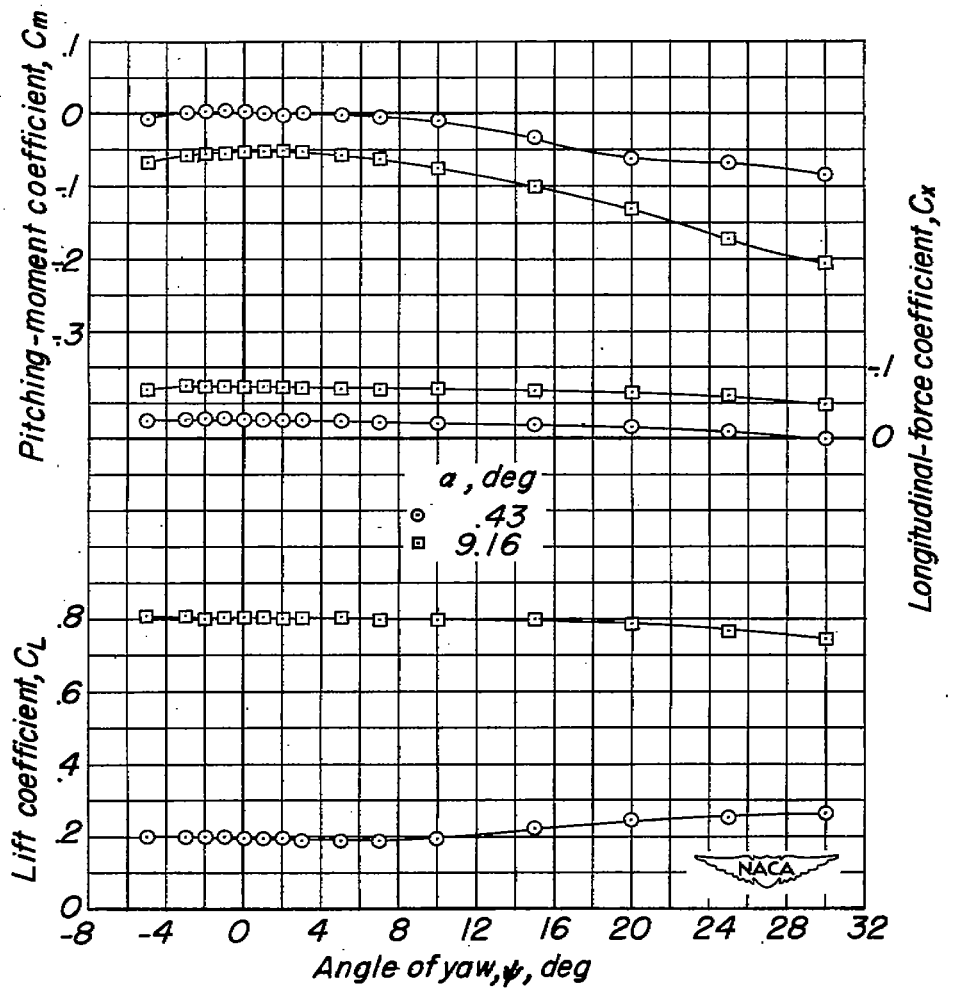

(b) Concluded.

Figure 19.- Continued.

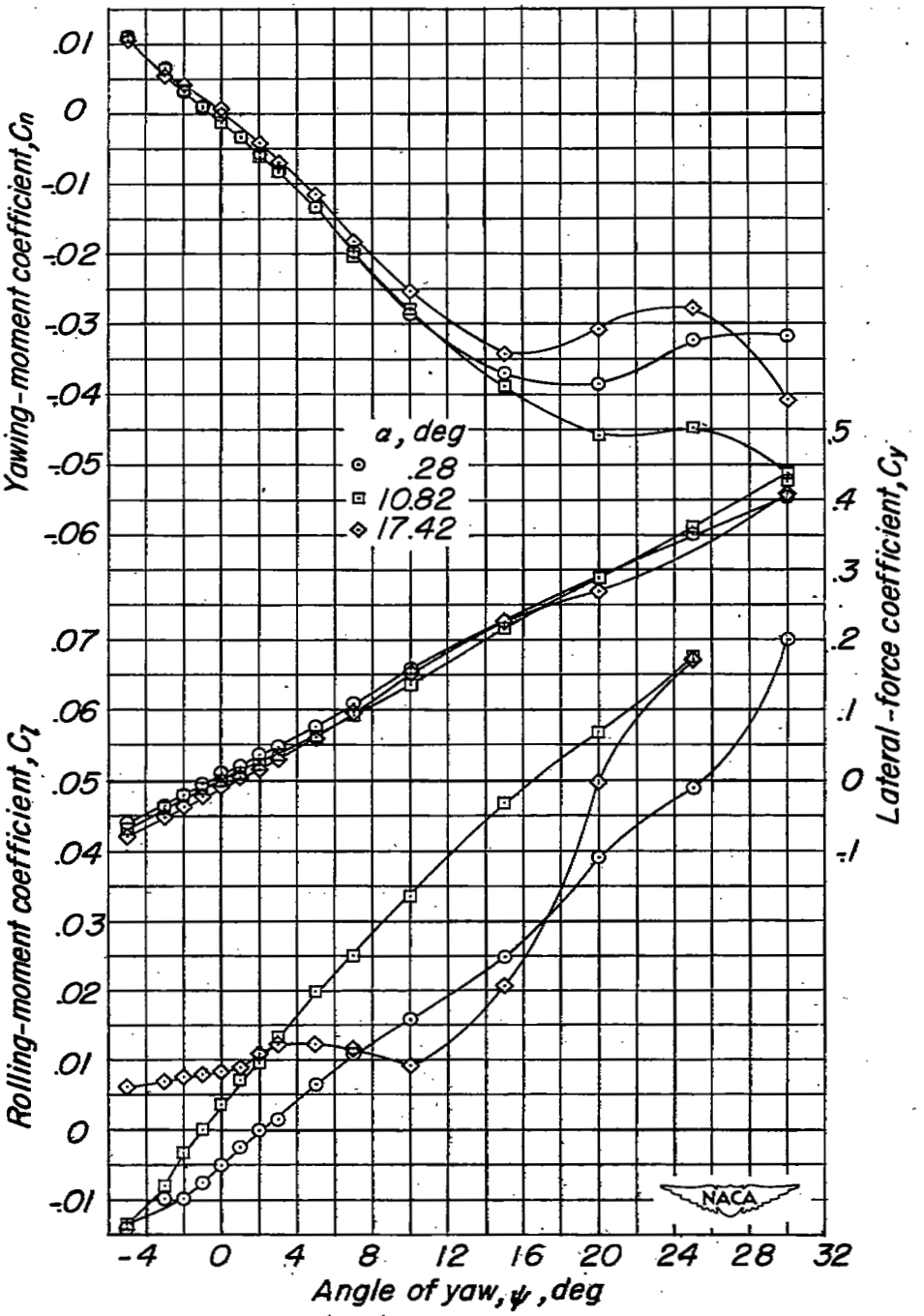

(c) $\Lambda = 50^\circ$.

Figure 19.- Continued.

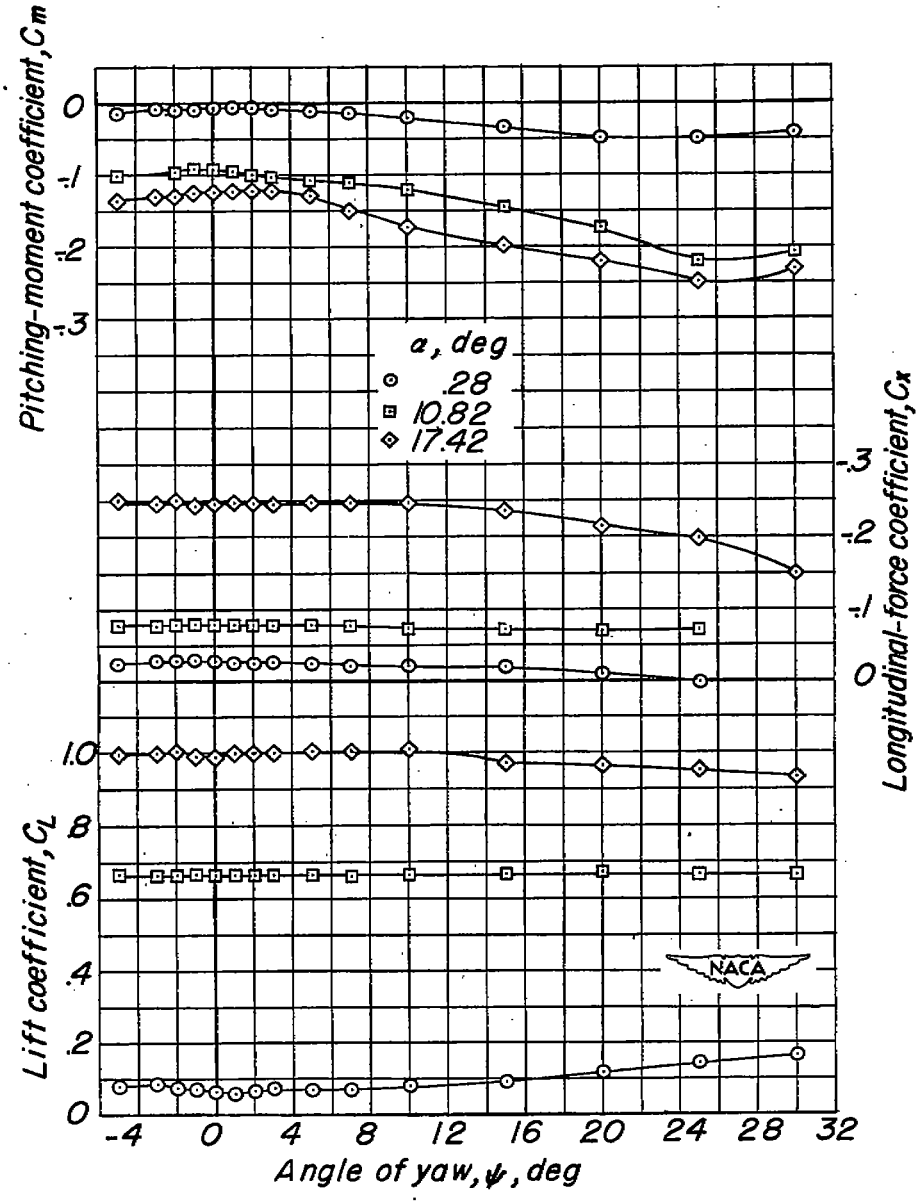

(c) Concluded.

Figure 19.- Continued.

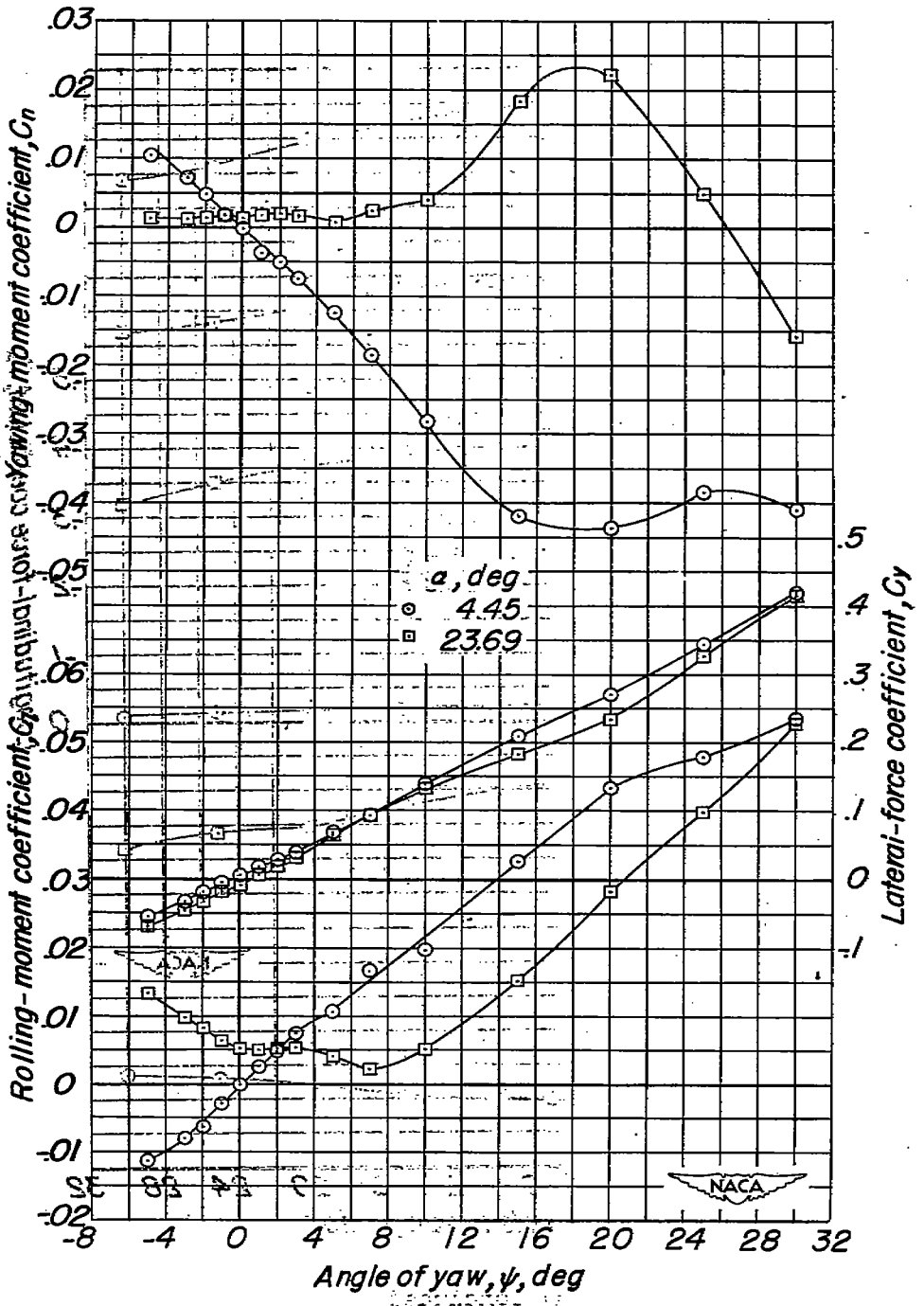

(d) $\Lambda = 60°$.

Figure 19.- Continued.

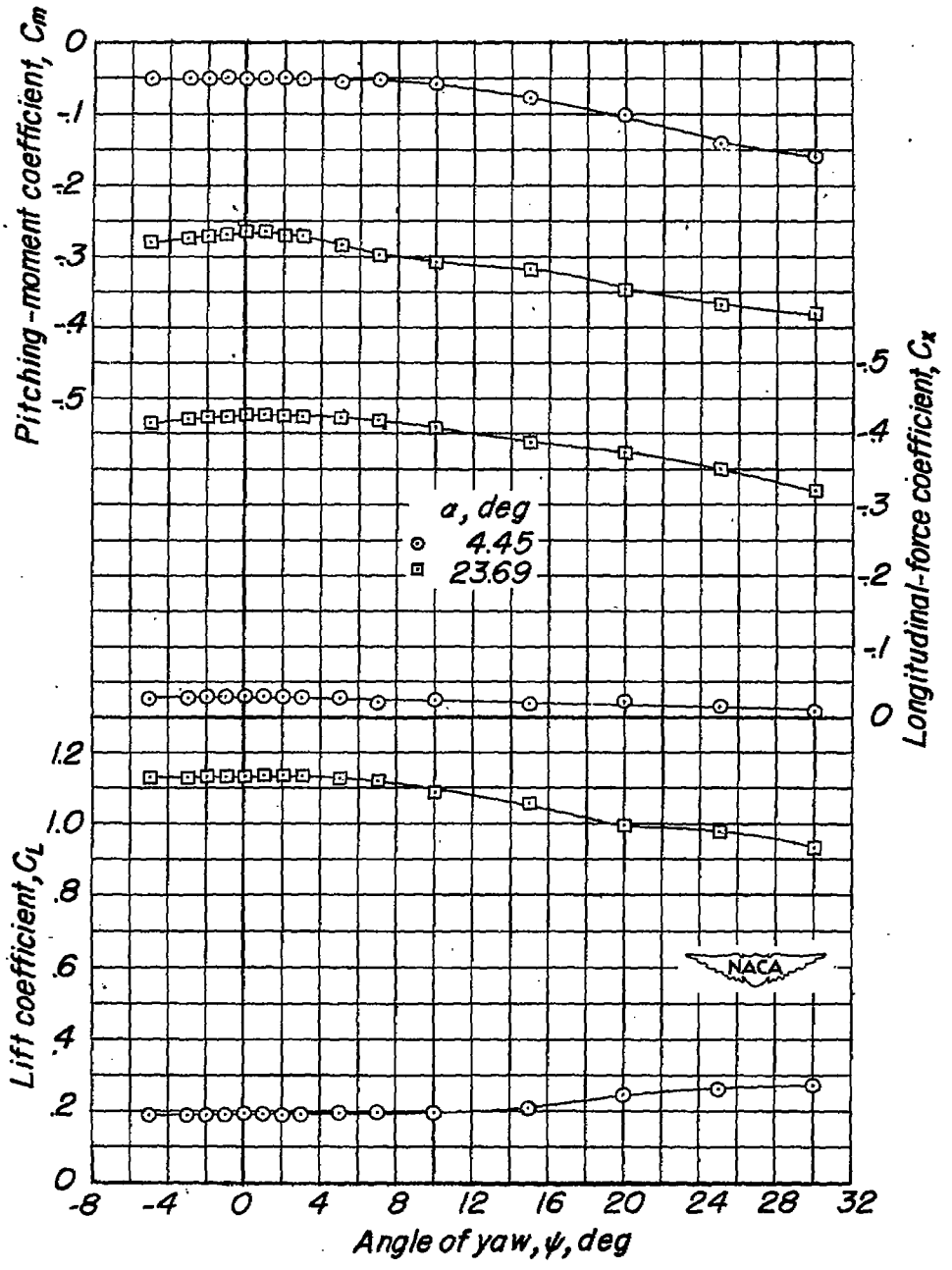

(d) Concluded.

Figure 19.- Concluded.

NACA-Langley - 2-1-52 - 325

[redacted]